8

Advanced Austenitic Heat-Resistant Steels for Ultra-Super-Critical (USC) Fossil Power Plants

Chengyu Chi[1,2], Hongyao Yu[2] and Xishan Xie[2]
[1]*School of Metallurgical and Ecological Engineering, University of Science and Technology, Beijing,*
[2]*School of Materials Science and Engineering, University of Science and Technology, Beijing, China*

1. Introduction

In recent years, construction of fossil-fired power plants with higher thermal efficiency has been speed up all over the world for meeting the large requirement of electricity with the rapid development of economy and continuous raising of people's living standard. With the promoting of steam parameters to USC(Ultra-Super-Critical) level even higher, high temperature materials with improved creep resistant strength, steam corrosion and oxidation resistance over 600℃ such as newly developed ferritic heat resistant steels, advanced austenitic heat resistant steels and Ni-base superalloys are required. Indeed the research and development of these high quality materials has become a key factor for USC power plants construction.

Nowadays, only advanced austenitic heat resistant steels are most suitable for USC power plants as the highest temperature components materials in the view of high temperature performance and cost. Mainly, there are three kinds of newly developed austenitic heat-resistant steels such as TP347H, Super304H and HR3C have been used as superheater/reheater tubes extensively all over the world(Viswanathan et al., 2005; Xie et al., 2010; Iseda et al., 2008; Hughes et al., 2003). In this chapter, thermodynamic calculation, SEM, TEM and Three Dimensional Atom Probe(3DAP) technology were used to analyze the microstructure evolution of these advanced austenitic heat-resistant steels during aging at 650℃ till 10,000hrs. The relationship of microstructure with age hardening effect and strengthening mechanism of these austenitic steels will be discussed. According to experimental results, the advice of further improvement of these austenitic heat-resistant steels will be also proposed.

2. Development of fossil-fired power plants

Thermal power generation boilers generate electricity by consuming fossil fuels such as coal, oil and liquid natural gas. It is generally recognized that fossil fuels and coal in particular will remain the primary energy source for electric power generation for many years(Gibbons, 2009). In this situation, for reducing the levels of CO_2 in the atmosphere and saving fossil energy, it is necessary to improve the efficiency of power generation. Especially

in many coal resource rich countries such as U.S., China and India, where fossil-fired power generation occupies the most important part in the structure of electricity supply. It is urgent to develop ultra-supercritial, high-efficiency coal-fired power plants to assure electricity supply safety and fossil resources effective use(Viswanathan & Bakker, 2001; Lin et al, 2009). United State was the first country to develop high efficiency USC steam generator technology in 1957, but it was ceased for a number of problems including superheater/reheater tube materials broke down(Masuyama, 2001). However, since the energy crisis broke out in the 1970s and the requirement of electricity with fast world economy growing was continually increasing, research to increase the efficiency of conventional fossil-fired power plants has been pursued worldwide. The need to reduce CO_2, SO_X and other environmentally hazardous gases emissions has recently provided another incentive to increase efficiency of fossil-fired power plants since the early of 1980s.

As well known, the efficiency of conventional fossil power plants is strongly affected by the steam temperature and pressure to reduce coal consumption and protect the environment. During the last fifty years steam parameters of fossil-fired power plants in the world have been gradually raised in program. Fig.1 shows the development of steam conditions of power plants in the world(Chen et al, 2007). It can be seen that the steam parameters of power plant is speed-up increasing and still aiming at higher level sponsored by new projects. For examples, the AD700 Project in Europe aims to build a demonstration plant operating with a main steam temperature of 700℃ in 2014 (or later time), and its estimated efficiency under these conditions will improve from 35% to nearly 46%, a 11% increase(Blum et al, 2004). Similarly, project sponsored by the U.S. Department of Energy has set 760℃ for advanced ultra-supercritical(A-USC) project as the goal by 2020(Viswanathan et al, 2006). In Japan, efforts to retrofit older units to enable operation at higher steam temperatures with higher efficiency. It parallels along with the Sunshine Program of setting 700℃ as the goal of steam temperature(Masuyama, 2005).

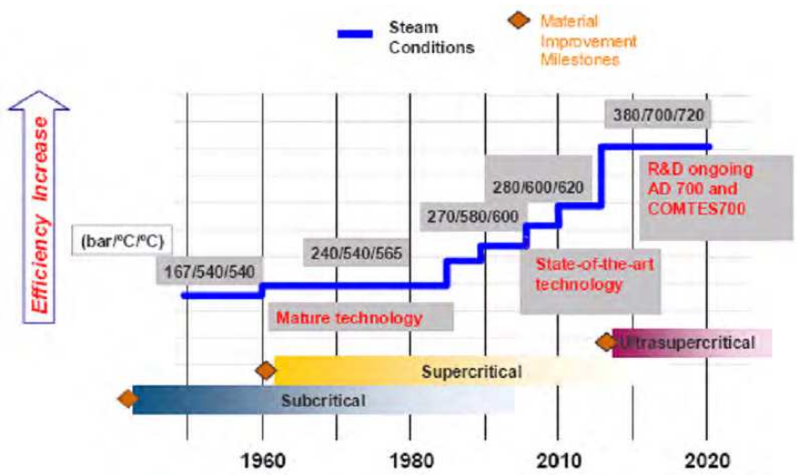

Fig. 1. Development of steam conditions in the world

It is also can be seen from Fig.1 that on every large steam parameters growing step there is always a material improvement. It means that invention of new materials with high performance promotes the improvement of fossil power plant technology. Although the

steam temperature will reach about 700℃ in the next 30 years (advanced ultra-supercritical technology), parameters of most power plants in the world recently still keep in the temperature range of 600-620℃ with the pressure of 27-28MPa, which belongs to USC power plant level. Nowadays, some high efficiency ultra supercritical(USC) power plants with 600℃ steam temperature have been built up and commercially operated all over the world, such as in USA, Germany, Denmark, Japan and China, which result not only in reduced fuel costs, but also reduced waste emission. It demonstrates that development of USC power plants is an effective way to achieve the aim of energy saving and environmental protection.

China also has a long history of fossil power plants development, and coal-fired power plants have occupied the main part in the structure of electricity supply and this situation will still keep for a long time. Recently Chinese government has announced to the world that CO_2 emission per GDP unit in 2020 would be decreased 40-45% in comparison with it in 2005. Chinese fossil power units have faced to a tough task to increase thermal efficiency and to decrease the emission of CO_2, SO_X and NO_X by means of shutting down small coal-fired power plants and developing ultra supercritical power units with high thermal efficiency. Fig.2 shows steam parameters evolution of Chinese coal-fired power plants(Liu et al, 2011). It can be seen that steam parameters of coal-fired power plants in China is increasing quickly. The first commercial operated USC unit with 26.25MPa/600℃/600℃ had been started since Nov.28 in 2006 at Zhejiang province in China. The thermal efficiency reaches 45.4% and the coal consumption decreases to 283.2g/kWh for 1,000MW unit at Yuhuan USC power plant, indicating that development of USC power plants can meet the requirement of economy development. Up to now, there are sixteen 1,000MW USC power plants and twenty-one 600MW USC power plants in operation or under construction, and installed USC units are 72 in sum, which need a large amount of high performance heat-resistant steels and alloys. With the promoting of steam parameters of advanced USC power plants to 700℃/40MPa even higher(shown in Fig.2), high temperature materials with requiring good performance should be a big issue to be faced.

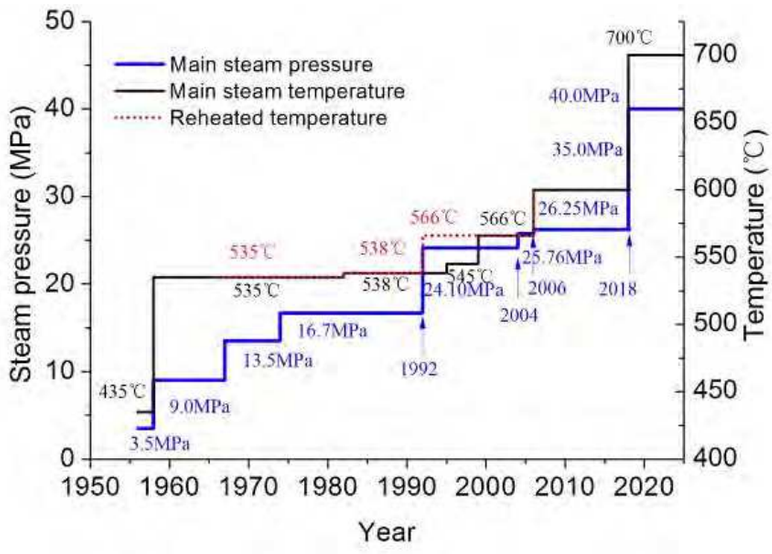

Fig. 2. Steam parameters evolution of Chinese USC power plants

There are many different components in USC power plants, such as water wall, superheater/reheater tube, header and main steam pipe need to use materials with excellent high temperature strength. However, superheater/reheater tubes are operated at the highest temperature range among these components. Therefore, the key issue to assure increase of steam temperature and pressure in boiler is the materials that will be used for superheater/reheater tubes, which must provide high creep rupture strength and high corrosion/oxidation resistance both at high-temperature conditions. Fig.3 shows the relationship of the allowable stresses and temperature for different type boiler materials(Viswanathan, 2004). Stress rupture data of these materials are dramatically decreased with the increasing of temperatures. It can be seem from Fig.3 that ferritic steels and advanced 9-12%Cr heat-resisting steels which has been widely used in conventional boilers can not be used for USC boilers with steam temperature higher than 600℃, because of its abruptly decreased allowable stress and relatively poor corrosion/oxidation resistance. Although Ni-base superalloys can meet the requirement both of high temperature strength and corrosion/oxidation resistance, however it is hard to be accepted because of its high price. Nowadays, only advanced austenitic heat-resistant steels with good high temperature performances and relatively lower cost are suitable to produce superheater/reheater tubes for 600℃ USC power plants.

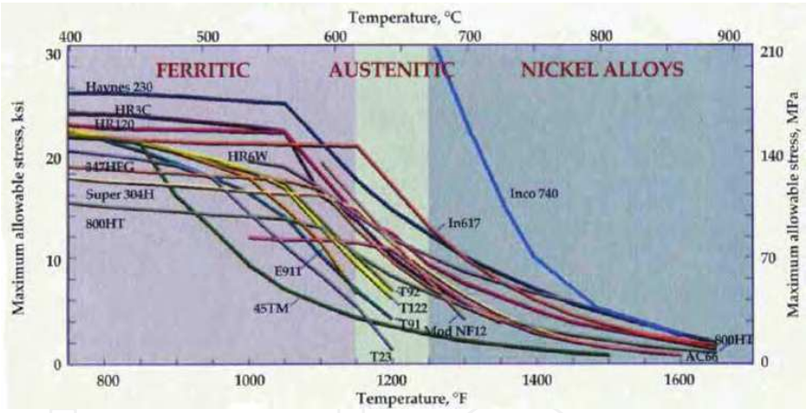

Fig. 3. Boiler materials for ultra-super critical coal-fired power plants

3. Development of austenitic heat-resistant steels

The service life of coal-fired power plants needs to reach 30~40 years. The material used for superheater/reheater tubes must be reliable over very long times at high temperatures and in severe environments. The main enabling technology is the development of stronger high-temperature materials capable of operating under high stresses at high temperatures. As mention in above paragraph, only new type austenitic heat resistant steels can be used as superheater/reheater tubes for 600℃ USC power plants on the view of high temperature performance. New type austenitic heat resistant steels are origin of 18Cr-9Ni austenitic stainless steel which was early chosen for high temperature components in the first USC power plant in U.S. However, it broke down because of its poor high temperature performance and the unit must be shut down. At the efforts to pursuing for high

temperature strength and good oxidation resistance by adding or optimizing alloying elements and increasing Cr, Ni content, conventional Cr-Ni austenitic steel has developed to modified 18Cr-9Ni type or 25Cr-20Ni type austenitic heat resistant steels(Yoshikawa et al, 1988; Sawaragi et al, 1992; Sourmail & Bhadeshia, 2005).

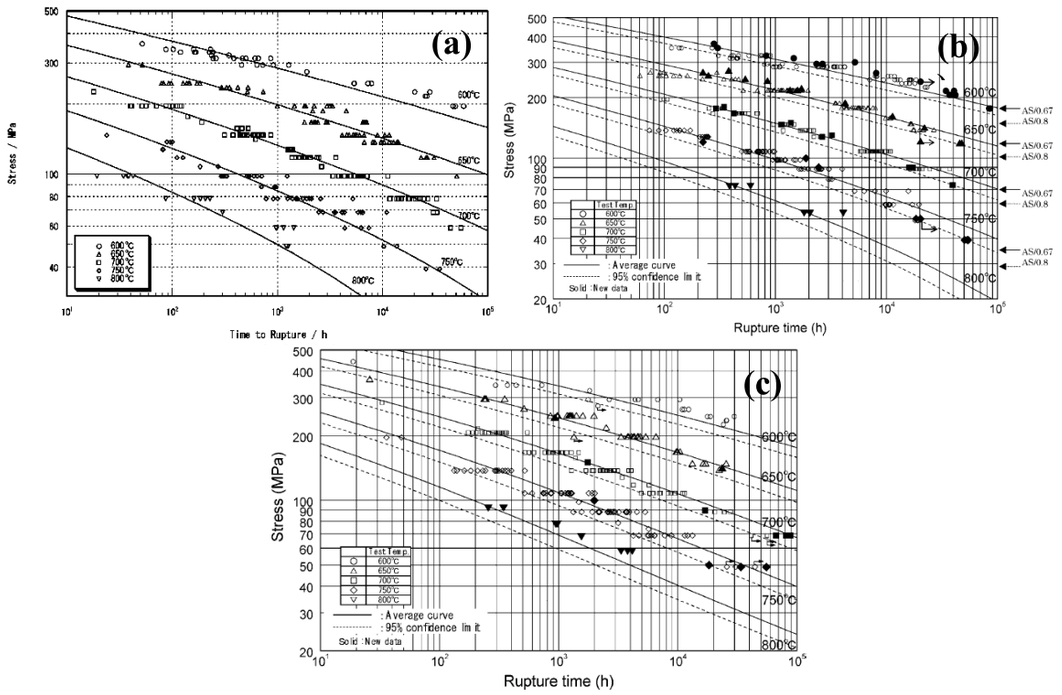

Fig. 4. Creep rupture data for TP347H(a), Super304H(b) and HR3C(c)

In order to improve high temperature creep rupture strength, not only solid solution strengthening elements such as W and Mo, but also precipitation strengthening elements such as Nb, Ti, V, are added to 18Cr-9Ni base austenitic steels to form carbon-nitrid MX for age hardening. Additionally, the element which can segregate at grain boundaries such as B is also added to increase grain boundary strengthening. The details information on improving austenitic heat resistant steel strength by alloying addition can refer paper(Masuyama, 2001). However, with the steam parameter increasing continually, 18Cr-9Ni type austenitic heat resistant steel can not burden the severe environmental corrosion and oxidation. Therefore, the Cr content has to increase to 25% and newly 25Cr-20Ni type austenitic heat resistant steel was invented. In recent 30 years researching several series of innovative austenitic heat resistant steels have been developed or in developing. Their chemical compositions are listed in Table.1. These austenitic heat resistant steels are all precipitation strengthening type steels by adding Nb element. Some steels also added W, Mo, V, N and B elements. Cu element is even added to some of these steels to further increase its creep rupture strength. Three typical newly developed austenitic heat resistant steels, TP347H, Super304H and HR3C, have been successfully serviced as superheater/reheater tubes in 600℃ USC power plants all over the world. Fig.4(a), (b) and (c) show creep rupture data for TP347H, Super304H and HR3C steels, respectively(Iseda et al., 2008). In comparison with these three creep rupture data, it can be seen that creep strength of Super304H at 650℃ is much higher than TP347H, and its long-term creep

strength is even slightly higher than HR3C. It shows that Super304H has better strengthening effect and more stable microstructure during high temperature long time service. So in order to deeply understand strengthening effect and its mechanism of these newly developed austenitic heat resistant steels, the microstructure evolution of these three typical austenitic heat resistant steels during 650℃ aging will be analyzed and comparatively discussed.

Steel	C	Si	Mn	Ni	Cr	Fe	Mo	W	V	Nb	Ti	Others
TP347H	0.08	0.6	1.6	10.0	18.0	Bal.	-	-	-	0.8	-	-
TempaloyA-1	0.12	0.6	1.6	10.0	18.0	Bal.	-	-	-	0.1	0.08	-
Super304H	0.1	0.2	0.8	9.0	18.0	Bal.	-	-	-	0.4	-	3.0Cu, 0.2N, 0.003B
XA704	0.03	0.3	1.5	9.0	18.0	Bal.	-	2.0	0.3	0.35	-	0.2N
SAVE 25	0.1	0.1	1.0	18.0	23.0	Bal.	-	1.5	-	0.45	-	3.0Cu, 0.2N
Sanicro 25	0.08	0.2	0.5	25.0	22.0	Bal.	-	3.0	-	0.3	-	3. 0Cu, 0.2N
TempaloyA-3	0.05	0.4	1.5	15.0	22.0	Bal.	-	-	-	0.7	-	0.15N, 0.002B
HR3C	0.06	0.4	1.2	20.0	25.0	Bal.	-	-	-	0.45	-	0.2N
NF709	0.02	0.5	1.0	25.0	22.0	Bal.	1.5	-	-	0.2	0.1	0.2N, 0.004B

Table 1. Nominal chemical compositions of typical austenitic heat resistant steels used or under development for superheater/reheater tubes in 600℃ USC power plants(wt%)

4. Typical advanced austenitic heat-resistant steels for superheater /reheater tubes

In this part the character of microstructure and strengthening mechanism in three austenitic heat resistant steels (TP347H，Super304H and HR3C) for 600℃ USC power plants have been compared according to the results of microstructure analyses and thermodynamic calculation. The microstructure of steels aging at 650℃ was observed by Scanning Electron Microscopy (SEM), Transmission Electron Microscopy (TEM) and Three Dimensional Atom Probe (3DAP) have been also used for detail analyses. The thermodynamic calculation results were obtained by using Thermo-Calc software.

4.1 TP347H heat-resistant steel

TP347H steel is a kind of traditional austenitic heat-resistant steels, which is used as superheater/reheater tube material. This kind of 18%Cr-9%Ni steel contains with about 0.7%Nb and it keeps higher allowable stress and creep rupture strength than TP304, TP321H and TP316H(Viswanathan, 2009). The chemical composition of TP347H steel for our research is as follows(in mass%): 0.07C, 0.35Si, 1.35Mn, 0.016P, 0.003S, 11.22Ni, 18.08Cr, 0.68Nb, bal. Fe. Steel was solution treated at high temperature of 1150-1200℃, then water quenched to prevent new phase precipitation during cooling. In order to investigate the change of precipitated phases with aging time, aging treatments were conducted from 1,000h to 10,000h at 650℃.

4.1.1 Long-term age hardening effect

The changes of tensile strength of TP347H steel after long-term aging at 650℃ are shown in Fig.5. The tensile strength increases quickly at the initial stage and has a peak value at

650℃/1,000h. The tensile strength stably keeps in a high level from 1,000h till 10,00h during 650℃ long-term aging. It is clear that TP347H characterizes with stable mechanical properties and age strengthening effect developed by strengthening phase precipitation.

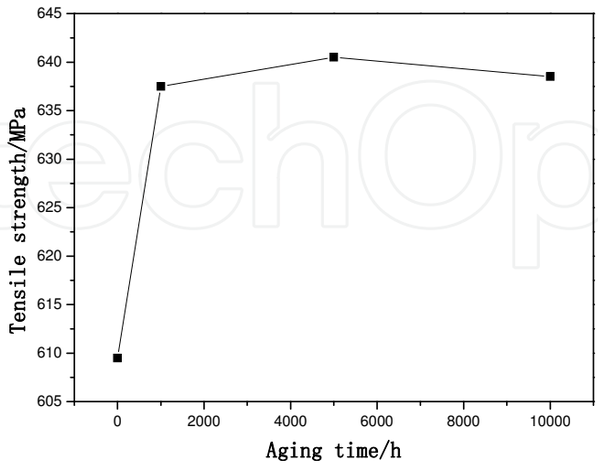

Fig. 5. Tensile strength of TP347H steel at 650℃ long-term aging

4.1.2 Micro-structure analyses

Micro-structure characterization of TP347H was analyzed firstly by means of scanning electron microscope (SEM). Fig.6 shows SEM images and EDS spectrum corresponding to the precipitates of TP347H steel at solid solution treatment condition and after 1,000h and 5,000h long-term aging at 650℃. Fig.6(a) and (b) are the SEM images at solid solution treatment condition. Some primary NbC inclusions randomly exist in the grains and also occasionally at grain boundaries and their size is about 1-3μm, shown in Fig.6(a) and (b). Fig.6(c) and (d) are the SEM images after 1,000h and 5,000h long-term aging at 650℃, respectively. Fig.6(e) is the EDS analysis result of the nano-size phase precipitated in grains shown by the arrow. This EDS spectrum shows that nano-size precipitate is rich in Nb and C, which indicates that the nano-size precipitate is MX type NbC phase. After long-term aging at 650℃, the amount of precipitates in grains increases intensively and there are also some Cr-rich precipitates($M_{23}C_6$ carbide) at grain boundaries, shown in Figure.6(c) and (d). The main precipitated phase in grains is Nb-rich(NbC) precipitates.

Transmission electron microscope (TEM) has been used for surveying nano-size particles. Fig.7 shows TEM images, diffraction patterns and EDS spectrum of TP347H austenitic heat resistant steel at solid solution treatment condition. There are some primary NbC carbide particles as inclusions and some undissolved MX phase in grains confirmed by diffraction pattern, shown in Fig.7(a) and (b). The size of primary NbC carbide is about 1-3μm which can directly form during solidification. The primary NbC inclusion is not good for strengthening during long-term creep, because of its large size and the cracks may happen nearby the inclusions and grow up quickly. The size of undissolved MX phase is about 300-600nm and most of them are spherical. Fig.7(c) and (d) show the EDS analysis of matrix and the undissolved MX phase, respectively. According to the diffraction pattern and EDS results, it can be known that the nano-size undissolved MX particle is Nb rich NbC phase.

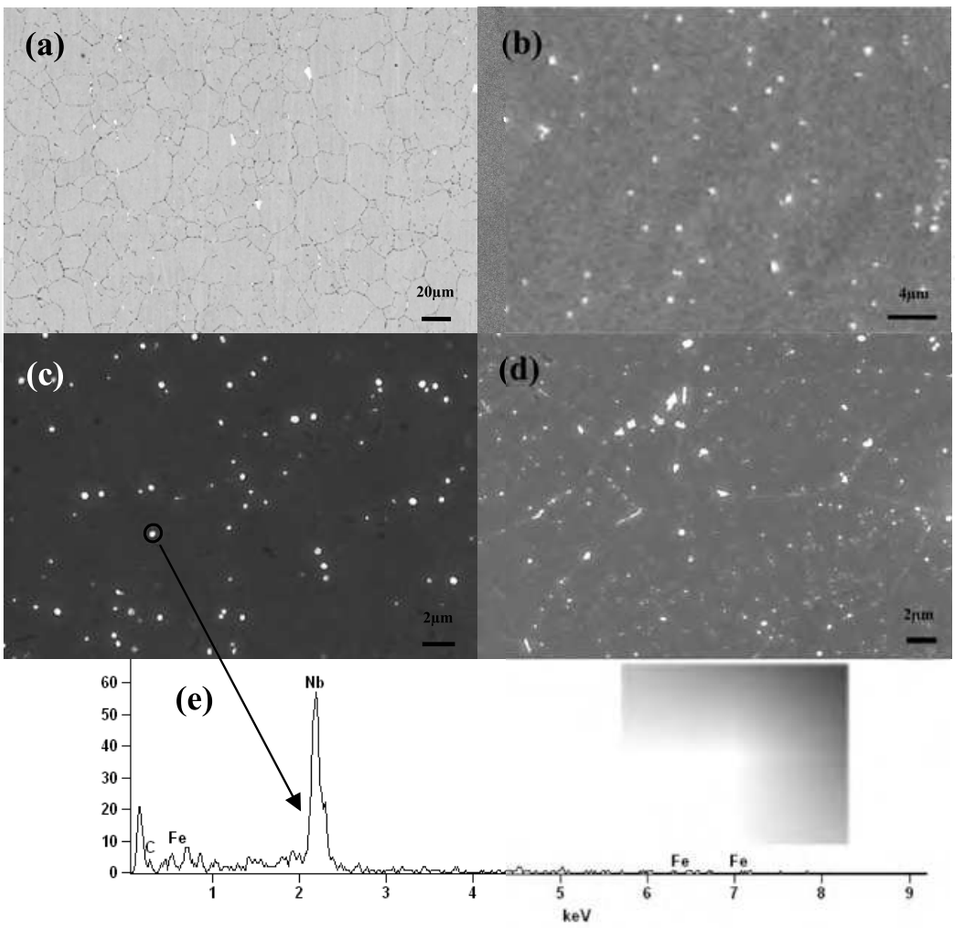

Fig. 6. SEM images of TP347H austenitic heat resistant steel after long-term aging at 650℃: solution treatment condition(a)(b), 650℃ aging for 1,000h (c), 5,000h(d), and EDS spectrum corresponding to the precipitates in the grain(e)

The TEM micrographs of TP347H austenitic heat resistant steel after 1,000h long-term aging at 650℃ is shown in Fig.8. During the initial aging, very fine nano-size MX phase with NaCl crystal structure precipitate in grains, as shown in Fig.8(b). Its size is about 28nm only. The morphology of MX is not spherical but in quadrate shape. $M_{23}C_6$ carbide can precipitate at grain boundaries when a solution-treated stainless steel is aged isothermally or slowly cooled within the temperature range of 500-900℃(Tanaka et al, 2001). The Cr-rich phase $M_{23}C_6$ carbide precipitates at grain boundaries of this steel, shown in Fig.8 (c). The corresponding EDS spectrum is shown in Fig.8(d). It shows that this Cr-rich precipitates at grain boundaries is $Cr_{23}C_6$ phase. The morphology of $Cr_{23}C_6$ is globular and keeps in chain-like distribution at grain boundaries after 650℃/1,000h aging. The size of grain boundary carbide $Cr_{23}C_6$ is about 100nm, which is much bigger than MX precipitates in grains. $Cr_{23}C_6$ carbide is very often found in the early stage of precipitation because it nucleates easily at grain boundaries. Incoherent or coherent twin boundaries and sometimes intragranular sites are all the nucleation sites of $Cr_{23}C_6$ carbide, but the most favorable sites for $Cr_{23}C_6$ carbide precipitation are grain boundaries(Hong et al, 2001). In this research, it is confirmed that $M_{23}C_6$ carbide mainly precipitates at grain boundaries.

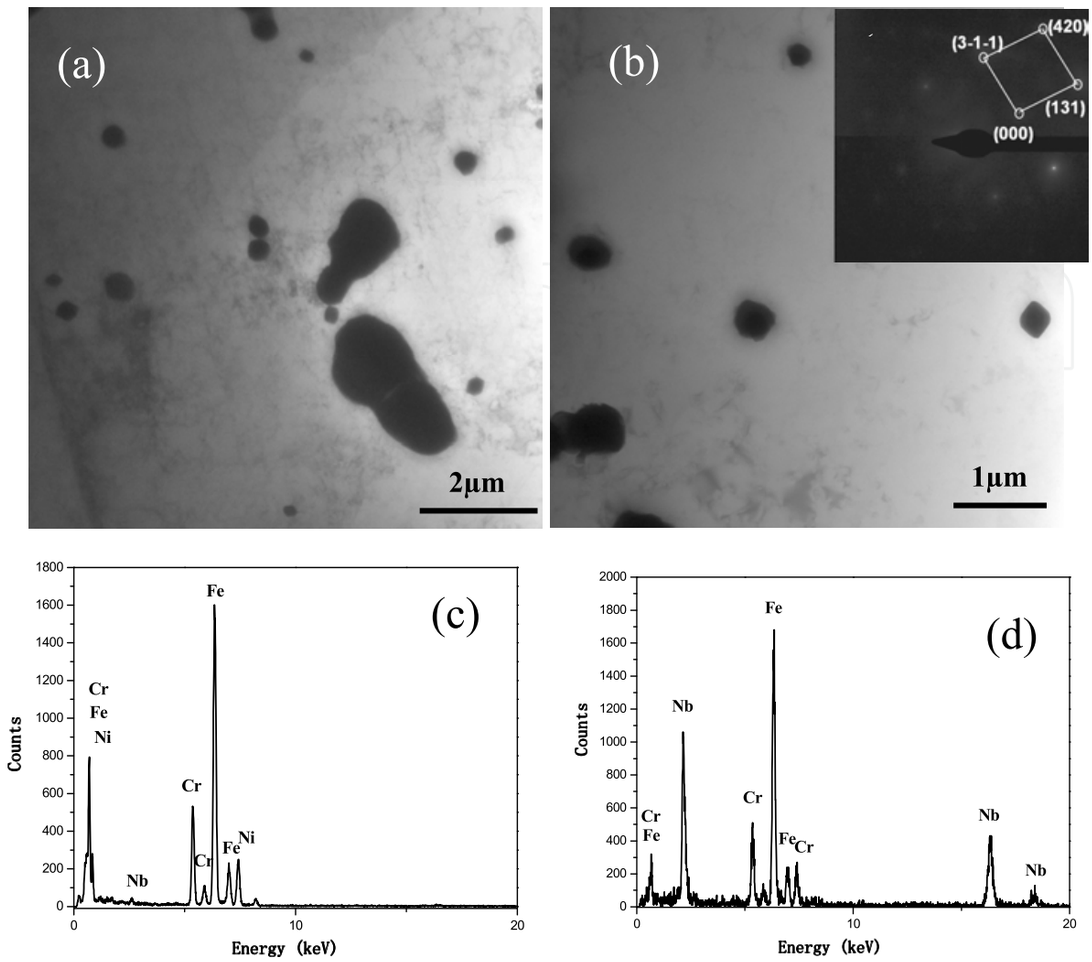

Fig. 7. TEM images of TP347H heat resistant steel after solution treatment (a) with diffraction pattern corresponding to the undissolved MX phase (b), EDS spectrum of the austenitic matrix (c) and the undissolved MX phase in grains (d)

After further long-term aging, the microstructures of TP347H austenitic heat resistant steel have changed. Figure.9 shows TEM images and diffraction patterns of precipitates in TP347H steel after 5,000h and 10,000h long-term aging at 650℃. Compared Fig.9(a) and (c) with Fig.8(b), it confirms that MX phase grows slowly. After 5,000h aging its size keeps in 35nm and even aging 10,000h its size still keeps in 50nm. Fig.9(d) shows the diffraction patterns of this nano-size particles and γ-matrix. It can be seen that the orientation relationship between MX phase and γ-matrix is $<-121>_{MX}//<1-1-2>_{\gamma}$. The lattice parameter of MX phase (a_{MX}) is 0.4421nm which is bigger than the lattice parameter of matrix phase (a_{γ}) 0.3635nm. Comparing Fig.8(a) and Fig.9(b), the density of the nano-size MX particle is increasing with aging time. The undissolved MX phase still exit after 10,000h long-term aging, shown in Fig.9(b). It can be seen clearly that there are two types of MX phase exited in the grains during long-term aging. One is the undissolved MX phase and its size keeps 300-600nm all the time. The other one is nano-size MX phase which precipitate during long-term aging and its growth rate is very slow. There is a very small amount of undissolved MX phase in the grains compared with precipitated MX particles.

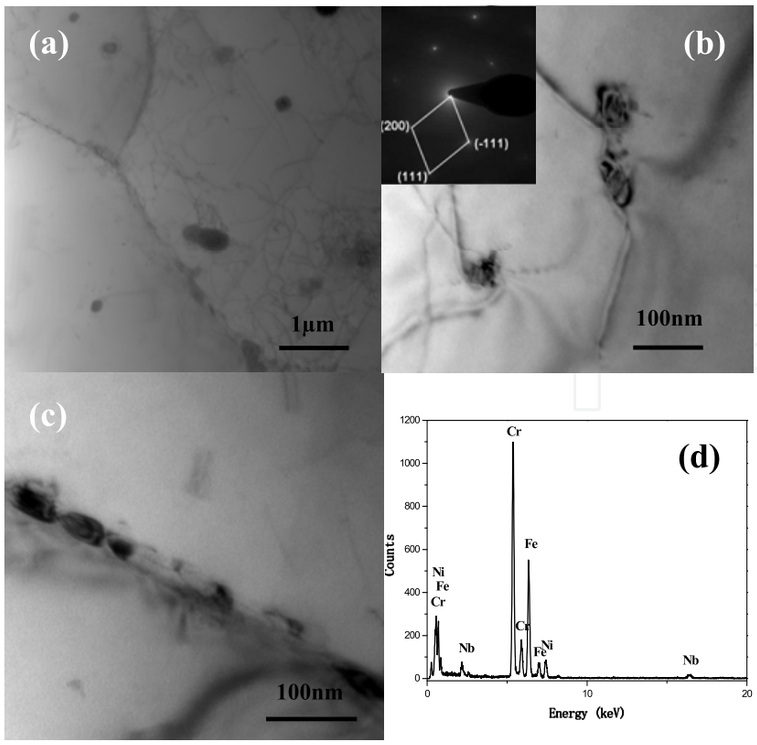

Fig. 8. TEM images of TP347H austenitic heat resistant steel after 1,000h long-term aging at 650℃ (a) with diffraction pattern corresponding to precipitation in grain (b), precipitation at grain boundary(c), and corresponding EDS spectrum(d)

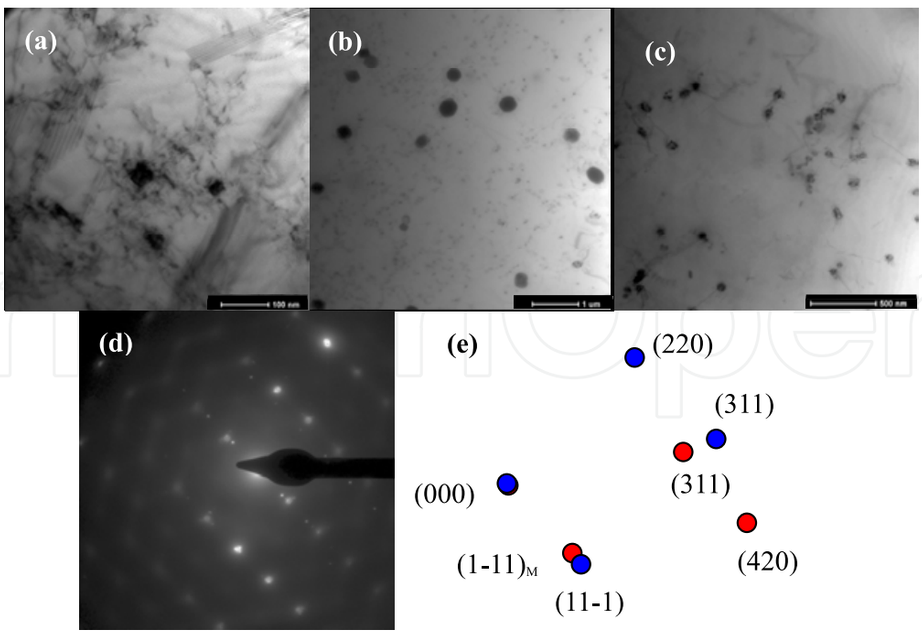

Fig. 9. TEM images and diffraction patterns of precipitations in TP347H steel after long-term aging at 650℃ (a) 5,000h; (b) and (c) 10,000h; (d) and (e) diffraction patterns of γ-matrix and precipitation in(c)

4.1.3 The relationship between thermal equilibrium phases and temperature in TP347H

The fraction, size, morphology and distribution of carbides/nitrides have a great impact on the strengthening effect of age-hardening steels. According to Fig.10(a) and (b), MX, $M_{23}C_6$ and Sigma phase are the equilibrium phases at 650℃ for TP347H austenitic heat resistant steel. Fig.10(b) shows $M_{23}C_6$ carbide solutes in austenite matrix at 840℃. At this temperature, the rest equilibrium phases are austenite and MX phase. The amount of MX phase decreases with increasing temperature. MX phase solutes in austenite matrix at 1340℃. It is clearly that MX phase is a very stable phase in this steel. It explains that bigger MX phase exits because MX phase can precipitate and grow up during hot working and undissolve at solution treatment condition. This phenomenon is also reported by T. Sourmail and R. Ayer(Sourmail, 2001; Ayer et al, 1992).

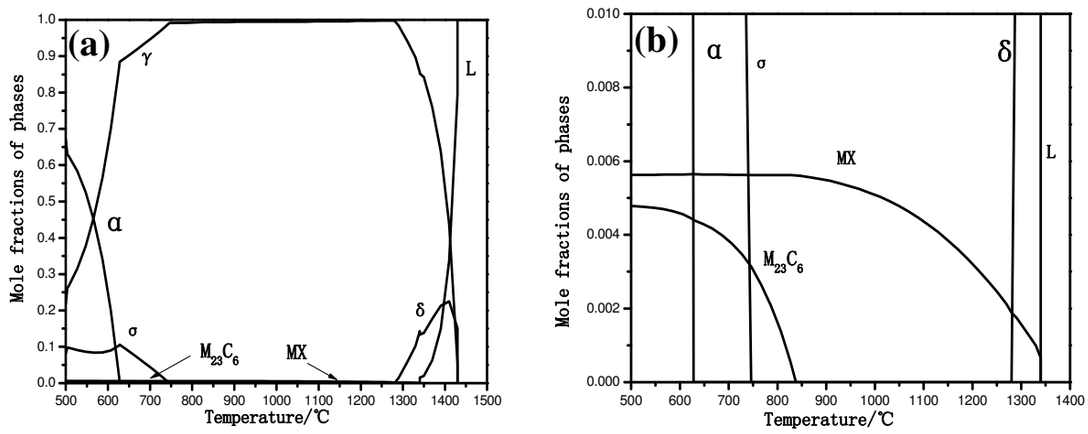

Fig. 10. Calculated mole fractions of phases on temperatures in TP347H steel (a) and its partial magnified diagram (b)

4.1.4 The relationship between thermal equilibrium phases and elements (C,N) in TP347H heat-resistant steel

According to the calculation results of Thermal-Calc., the main equilibrium precipitates are MX, $M_{23}C_6$ and Sigma phase. MX contains with Nb and C and $M_{23}C_6$ carbide contains with Cr, Fe and C. It also can confirm that the precipitation of carbides, especially nano-size MX in grains, plays the most important strengthening effect on creep rupture strengths according to experimental observation described in above paragraph. In order to optimize chemical composition of TP347H austenitic heat resistant steel with high creep rupture strength. Thermal-calc software has been used to predict the effect of MX containing elements C and Nb on the fraction of MX strengthening phase. The results are shown in Fig.11(a) and (b), respectively.

Fig.11(a) shows the effect of C content on mole fractions of MX phase. From 500℃ to 730℃ the content of C increases from 0.02% to 0.06%, the mole fraction of MX phase increases intensively. The C content increases 0.02%, the solution temperature of MX phase increases 60-80℃. However, when the content of C increases to 0.1%, the mole fractions of MX phase

do not increase obviously. It can be seen that the fractions of MX phase increases with the C content till 0.06%C at service condition (600-650℃). When the C content increases from 0.06% to 0.1%, the mole fractions of MX phase keep in a same level. Thus, the C content should be controlled in the level of 0.06%-0.07% C.

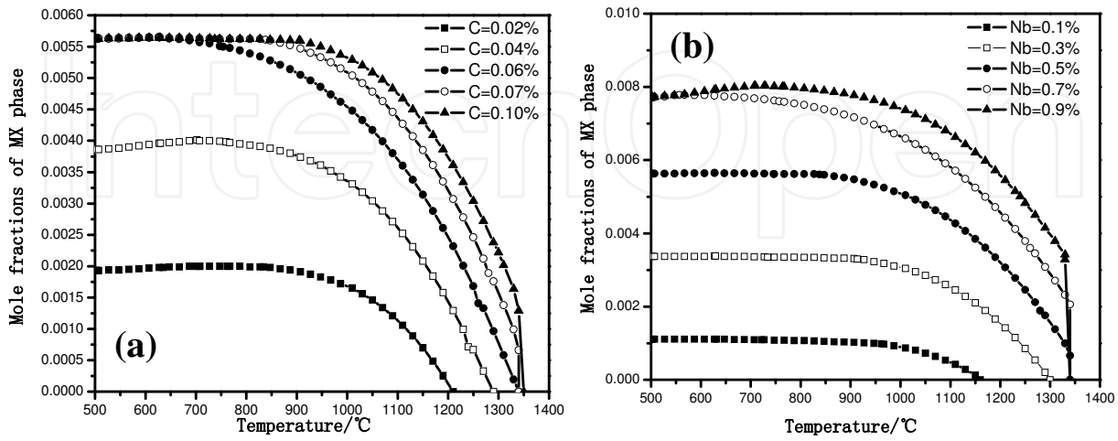

Fig. 11. Effect of C(a) and Nb(b) content on mole fractions of MX phase in TP347H

Fig.11(b) shows the effect of Nb content on mole fractions of MX phase. With the content of Nb increasing from 0.1% to 0.7%, the mole fractions of MX phase increase obviously. However, when the content of Nb increases to 0.9%, the mole fractions of MX phase do not increase obviously. Thus, the content of Nb should be controlled at about 0.7% for good strengthening effect of MX precipitation.

It is reported that the brittle σ phase can precipitate after long-term service in 18Cr-9Ni austenitic steels and it will cause mechanical property degredation(Minami et al, 1986). This research gave some results on σ phase. Fig.12 shows the effect of C content on the mole fractions of σ phase. The mole fractions of σ phase decrease obviously with the content of C increasing from 0.02% to 0.06%. Especially, when the content of C increases to 0.10%, the mole fractions of σ phase decrease quickly. Thus, the content of C should be controlled at high level to decrease the mole fractions of σ phase for good strengthening effect.

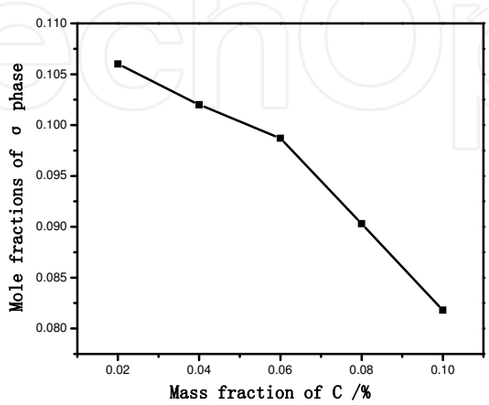

Fig. 12. Effect of C content on mole fractions of σ phase in TP347H steel at 650℃

The yield strength could increase from 229MPa to 238MPa with a certain amount of N element was reported in the literature(Ayer et al, 1992). The elongation of this steel with a certain amount of N element also increases. If this steel contains a certain amount of N, the complex carbonitride(MX) which contains with Nb, Cr, N and C forms and it can promote strengthening effect. This is why the mechanical properties of TP347H containing with N are increased. Nitrogen element can also play a good role in solid solution strengthening. Thus, to add a certain amount of N in TP347H steel will get better mechanical properties.

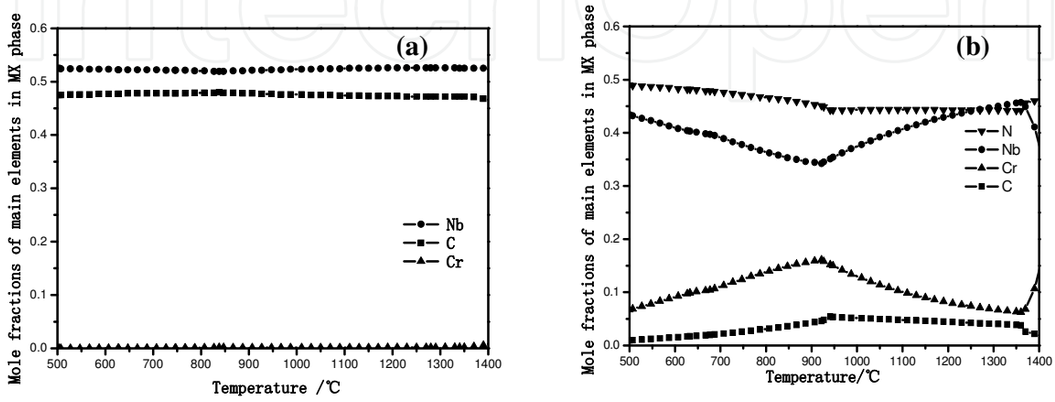

Fig. 13. Effect of N content on mole fractions of elements in MX phase for TP347H steel N= 0% (a) and N= 0.2%(b)

Fig.13 shows the effect of N content on mole fractions of elements in MX phase for TP347H steel. Fig.13(a) is the experimental steel without N and Fig.13(b) is the steel with 0.2%N. When there is no N in steel, Nb and C are the main elements in MX phase and their atomic ratio is 1:1. At this time MX phase is the simple niobium carbide(NbC). While the steel containing with 0.2%N, MX phase contains not only Nb and C but also Cr and N, which is a complex carbon-nitride. The mechanical properties can be increased by adding N in TP347H.

4.2 Super304H heat-resistant steel

Super304H steel belongs to 18%Cr-9%Ni system austenitic stainless steel, which has been added copper (Cu), niobium (Nb) and nitrogen (N) for precipitation strengthening. It is resulted in a good combination of elevated temperature creep strength and corrosion resistance(Sawaragi & Hirano., 1992; Sawaragi et al., 1994). Especially it has more than 20% higher stress rupture strength at 650℃ than TP347H which is conventionally used as superheater/reheater tube material(Muramatsu, 1999). The resistance to oxidation and corrosion of Super304H is superior to TP321H at high temperatures(Igarashi, 2004). It makes Super304H heat resistant steel to be an very effective austenitic heat resistant steel and has been widely accepted for the application of superheater/reheater tubes in boilers of USC power plants all over the world(Senba et al., 2002). The application of Super304H in USC power plants confirms its good high temperature performance and stability, which is important to be used in USC boilers(Igarashi et al., 2005; Komai et al., 2007). Cu addition is its distinct character compared with other austenitic heat resistant steels, which also causes

its good performance. This part attempts to provide the detail precipitation behavior and strengthening mechanism of Cu-rich phase in Super304H steel during long-term aging process at 650℃.

The chemical composition of investigated Super304H steel is as follows(in mass%): 0.08C, 0.23Si, 0.80Mn, 0.027P, 0.001S, 9.5Ni, 18.51Cr, 2.81Cu,0.51Nb, 0.11N, 0.0034B, bal. Fe. Its heat treatment is same with TP347H that is also solid solution treated at 1150℃ high temperature. In order to examine long-term precipitation behavior, aging treatments at 650℃ were conducted from 1h to 10,000h.

4.2.1 Long-term age hardening effect

Fig.14 shows the micro-hardness change in grains of Super304H aged at 650℃. After high temperature solid solution treatment, the value of micro-hardness is only 185HV. However, micro-hardness increases rapidly just from the very beginning of aging till 1,000h and at that time the highest micro-hardness value has gained at about 245HV. This value of micro-hardness is much higher than the micro-hardness of solid solution treatment condition. The micro-hardness of Super304H steadily keeps at high value about 240HV till 8,000h. It shows a very effective hardening effect during 650℃ aging.

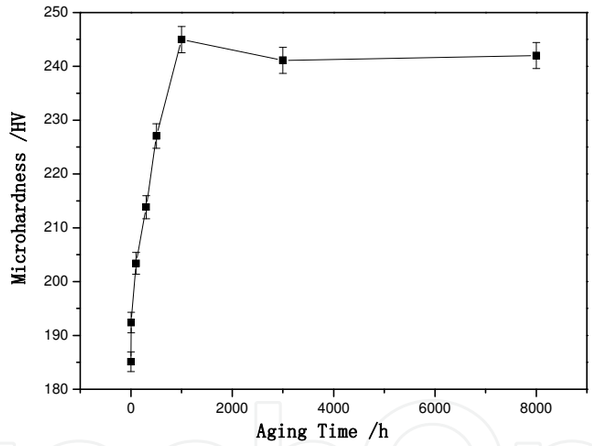

Fig. 14. The changes of micro-hardness in grain of Super304H after 650℃ long time aging

4.2.2 Tensile property after long-term aging

The room temperature ultimate tensile strength of Super304H after 650℃ long time aging keeps a similar tendency as micro-hardness change, as shown in Fig.15. The ultimate tensile strength also increases rapidly just from the very beginning of aging. Its value keeps around 700MPa till 10,000hrs after reaching the highest value. Although the room temperature ultimate tensile strength is increasing with aging time, the plasticity of aged steels does not drop sharply. The results of micro-hardness and ultimate tensile strength both indicate that some precipitates are forming to make an excellent hardening effect during 650℃ long time aging of Super304H.

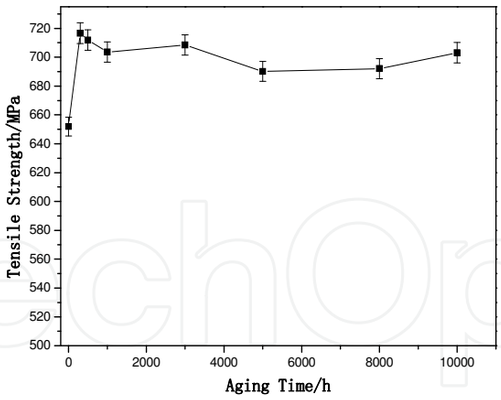

Fig. 15. The changes of ultimate tensile strength of Super304H after 650℃ long time aging

4.2.3 Micro-structure analyses by SEM and TEM

In order to study this unique age hardening effect, microstructure changes of aged samples have been detailed analyses by SEM and TEM. Typical SEM images of Super304H after aging for different times are shown in Fig.16. Fig.16(a) is the SEM image of Super304H just after solid solution treatment. Its microstructure characterizes with equiaxed austenite grains and with a few coarse and fine particles also. The coarse particles, which are in the size range of 1 to 3μm, as inclusions directly formed during solidification, randomly distributed in grains and partially at grain boundaries. There are also some spherical undissolved small particles distributed in grains with the size of about 0.1μm. Energy-dispersive spectroscopy(EDS) analysis reveals that two kinds of particles both mainly contain with niobium, they are niobium carbonitride directly formed during solidification and undissolved Nb(C,N) carbonitride respectively, which are similar to the two kinds of MX type phases existed in TP347H austenitic steel at solid solution condition.

Fig.16(b), (c) and (d) represents the SEM images of Super304H after exposure at 650℃ for 500, 5,000 and 10,000hrs, respectively. There are almost no precipitates at grain boundaries except larger niobium carbonitride just after solid solution treatment(see Fig.16(a)). The grain boundary precipitates contain with high content of Cr identified by EDS and also a few of particles in the grains are $M_{23}C_6$ carbide as shown in Fig.16(b) after 650℃ aging for 500h. Fig.16(c) shows that the size of $M_{23}C_6$ at grain boundaries is about 0.5μm and has contacted to each other to form chain-like precipitates after 650℃/5,000h ageing. Fig.16(d) shows the fine precipitates in grains which are rich in Nb detected by EDS. These precipitates are suggested as Nb rich MX phase. The size of MX precipitates is about 70nm when aged at 650℃ for 10,000h. SEM images can not find very fine precipitates except primary MX phase, undissolved small size MX phase after solid solution treatment and nano-size secondary MX phase precipitate in grains and $M_{23}C_6$ phase at grain boundaries during long-term aging. This result is similar to TP347H steel. However, the high temperature performance of Super304H is higher than TP347H steel, which means there must be some other precipitated strengthening phase in Super304H that is different from the precipitates in TP347H. For the purpose of detail study on precipitation hardening behavior of Super304H at 650℃ aging, TEM and 3DAP have been used to do more detail observation.

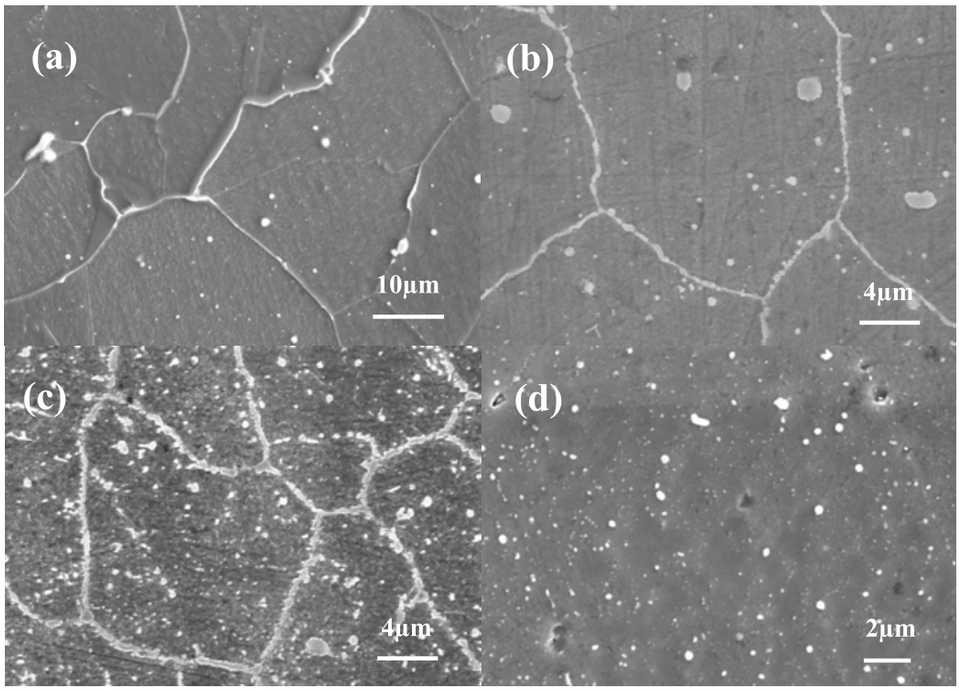

Fig. 16. SEM images of Suepr304H after solid solution treatment(a), aging at 650℃ for different times 500h(b), 5,000h(c) and high magnified image in grain aging for 10,000h(d)

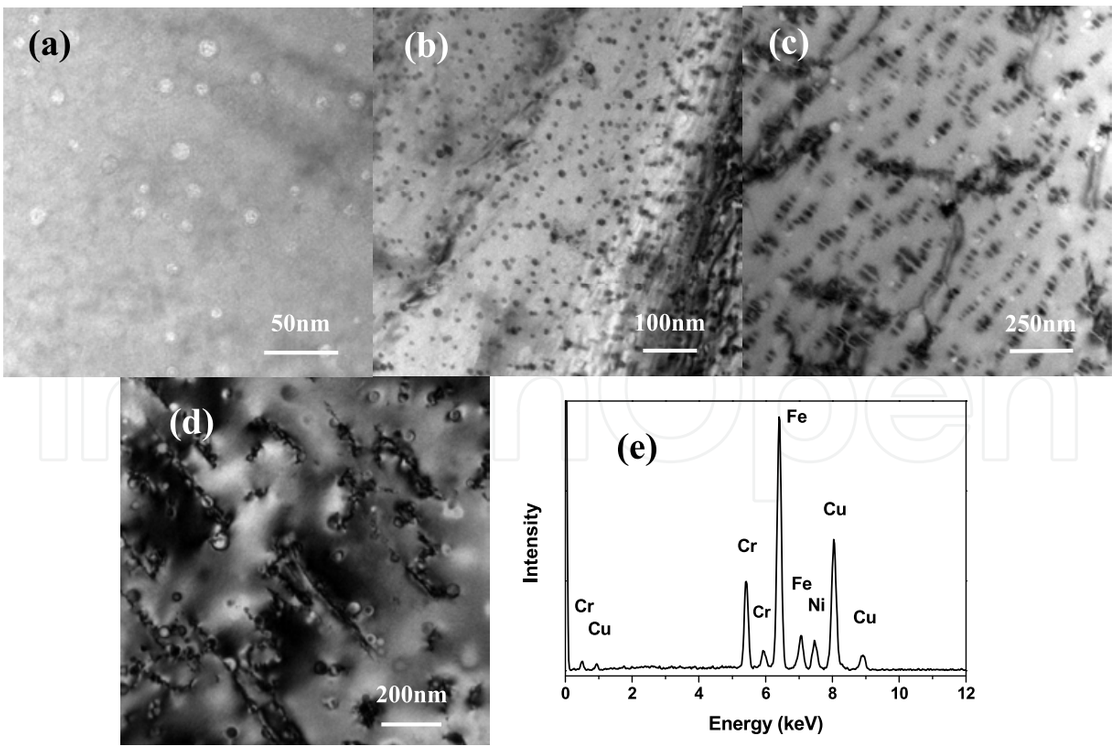

Fig. 17. TEM images of Super304H heat resistant steel aged at 650℃ for 500h (a), 1,000h (b), 5,000h (c), 10,000h (d) and EDS spectrum for Cu-rich phase(e).

Fig.17 shows the TEM images of Super304H aging at 650℃ for different times. Fig.17(a) is the TEM image of the sample aged at 650℃ for 500h. It shows that there are dense distribution of nano-size spherical precipitates in grains which contain high content of Cu determined by EDS spectrum as shown in Fig.17(e). It confirms that these nano-size precipitates are Cu-rich phase. Cu-rich phase has been clearly found by TEM during long-term aging at 650℃ for 1,000h as shown in Fig.17(b). The average size of Cu-rich phase is about 10nm only, and it distributes homogeneously with a higher density than MX phase. Because the size of Cu-rich phase is very fine and the lattice parameter of Cu(3.6153Å) is close to γ-matrix(3.5698Å), the diffraction pattern of Cu-rich phase is hard to be separated from γ-matrix. However, the images of spherical precipitate particles are separated into two parts by no-contrast line shown in Fig.17(c). It shows that Cu-rich phase is coherent with γ-matrix even aged at 650℃ for 5,000h. After aging for 10,000h, the Cu-rich phase still keeps nano-size(as shown in Fig.17(d)). At this time, it can be clearly seen from Fig.17(d) that dislocations contact with Cu-rich phase particles and are effectively blocked by Cu-rich phase. It indicates that these fine Cu-rich phase particles distribute uniformly with high density in grains are the main strengthening phase which can cause strong age hardening effect and supply excellent high temperature strength for Super304H steel, which has been reported by Yu(Yu et al., 2010).

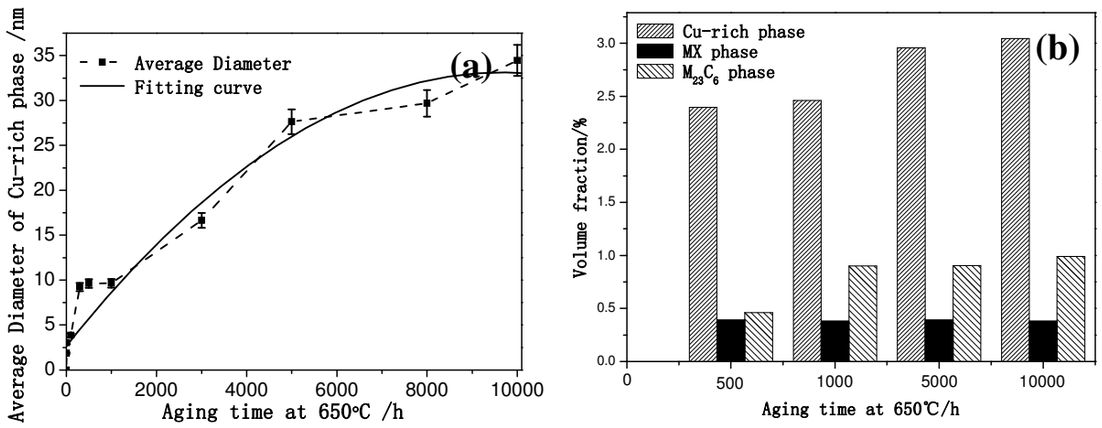

Fig. 18. The change of Cu-rich phase average diameters (a) and precipitates volume fraction (b) in Super304H at 650℃ with aging time

The Cu-rich phase is growing during 650℃ long time aging till 10,000hrs, but the growth rate is very slow. The average diameters change of Cu-rich phase has been determined by TEM as shown in Fig.18(a). This curve confirms that Cu-rich phase grows slowly at 650℃ long time aging. The average size of Cu-rich phase still keeps about 34nm at 650℃ aging for 10,000h. Experimental results confirm that Cu-rich phase and MX phase precipitate in grains, while $M_{23}C_6$ phase mainly precipitates at grain boundaries. The volume fractions of these phases change with aging time is shown in Fig.18(b). The volume fraction of MX is the sum of undissolved MX at solid solution treatment condition and secondary MX precipitates during long-term aging. It is stable and increases slightly during aging time. The volume fraction of Cu-rich phase increases gradually with aging time and its fraction is the highest in these three phases. It is clear that nano-size Cu-rich phase with the highest volume fraction and homogeneously distribution plays a very important role for strengthening

effect in Super304H steel. However, Cu-rich precipitates are so fine that hardly to be clearly detected by TEM. So three dimensional atom probe(3DAP) has been used to study the precipitation behavior of Cu-rich phase.

4.2.4 Cu-rich phase investigation by means of 3DAP technology

3DAP can effectively detect the nano-size precipitates by analyzing atoms reconstruction. Fig.19 shows the elements mapping of Super304H after solid solution treatment. The analyzed volume is 10nm×10nm×70nm. In these figures, one point represents an atom. From Fig.19 it is confirmed that all atoms have solved in austenitic matrix and homogeneously distributed at solid solution condition. There are no any traces of precipitate formation after high temperature solid solution treatment.

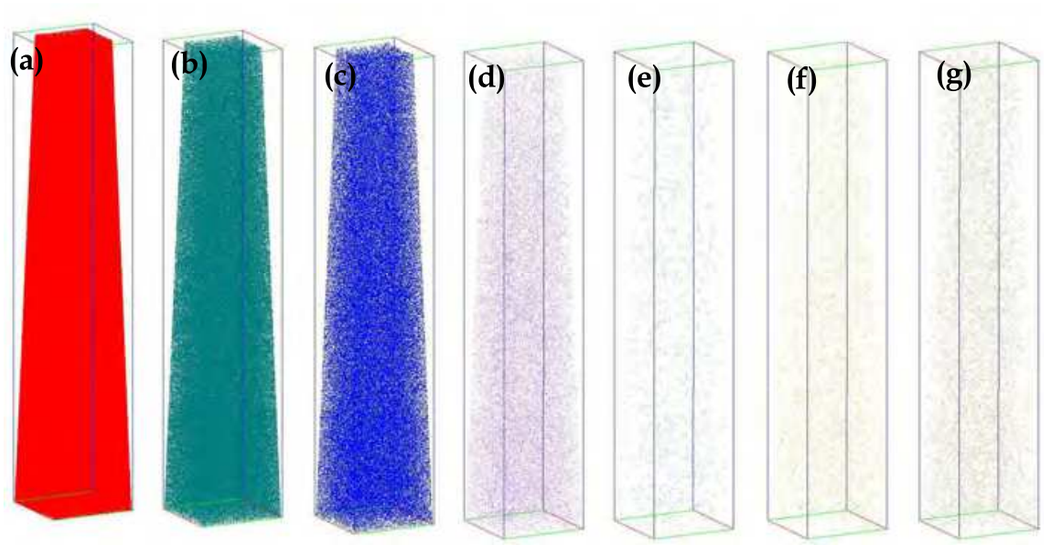

Fig. 19. Atomic mapping of the Super304H after solution treatment: Fe(a), Cr(b),Ni(c),Cu(d),Nb(e),C(f) and N(g)(size of selected box is 10nm×10nm×70nm)

Fig.20 shows the Cu atomic mapping of Super304H aged for different times. Fig.20(a) shows that Cu atoms continuously concentrate in clusters(about 1.5nm in radius) just at the beginning of aging treatment, which homogeneous distribute in austenitic matrix after 650℃ aging for 1h only. The average size of Cu-rich phase particles is increasing while the density of its distribution is decreasing with aging time(see Fig.20(b) and (c)). The density of Cu atoms in austenitic matrix is also slightly decreasing with aging time. It means that Cu atoms diffuse from matrix and concentrate into Cu-rich areas. This diffusion control process is continuing during Cu-rich phase growing process. When aged till to 1,000h the one Cu-rich particle is larger than above mentioned analyzed volume and is partially intercepted. However, this size is still very small and radius of this Cu-rich particle is about 3nm as shown in Fig.20(d). The Cu-rich phase particle density calculated according to the reference(Chi et al., 2010) is still very high and keeps at the level of 0.07×10^{24}n/m^3. These important results show that Cu-rich phase can keep a level of nano-size and high density distribution at 650℃ aging till 1,000 hrs.

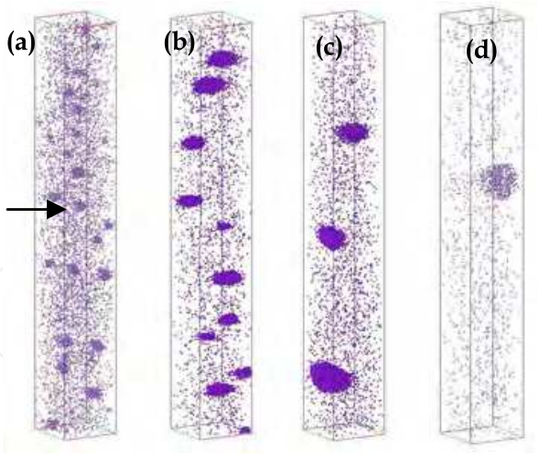

Fig. 20. Cu atomic mapping of Super304H aged for 1h(a), 100h(b), 500h(c) and 1,000h(d) at 650℃ (size of selected box is 10nm×10nm×70nm)

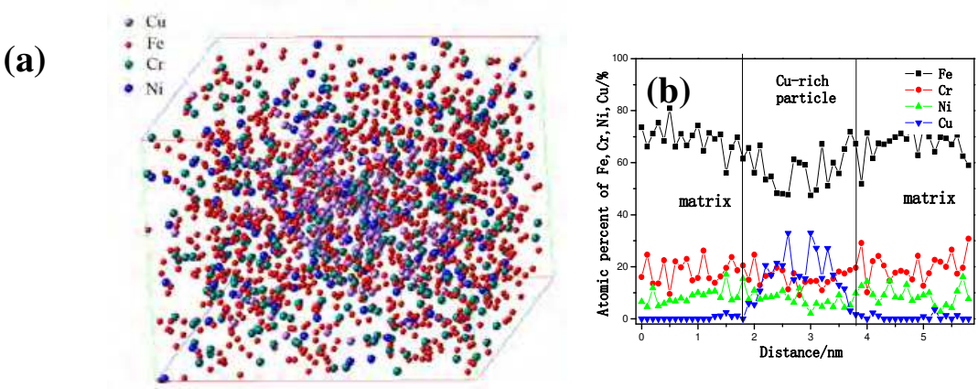

Fig. 21. 3DAP reconstruction map of a Cu-rich segregation area selected from Fig.20(a) as shown by the arrow (size of selected box is 3.5nm×3nm×2nm) (a); and a concentration depth profile through a Cu-rich segregation area and adjacent γ-matrix of the sample aged at 650 ℃ for 1h(b)

In order to detect the Cu atom composition concentration in Cu-rich phase, just one particle selected from 1h aged specimen(as shown in the Fig.20(a) by the arrow) was analyzed and the concentration profile of Fe, Cr, Ni and Cu through the Cu-rich phase particle is shown in Fig.21. Fig.21(a) shows that the Cu-rich particle is composed of Cu ,Fe, Cr and Ni, which indicates a certain degree of Cu atom concentration when aged at 650℃ for 1h only. The concentration depth profile through the Cu-rich segregation area is shown in Fig.21(b). It can be seen that the composition profiles are asymmetric across adjacent γ -matrix and Cu-rich particle two interfaces. Although the boundary between Cu-rich segregated particle and austenitic matrix is fluctuant, Cu compositions undergo a sharp transition across the Cu-rich particle and austenitic matrix interface. The Cu atom concentration is increasing from the edge to the centre of Cu-rich segregation area and reaches the highest degree in the centre of Cu-rich segregation area, while the others composed atoms such as Fe, Cr and Ni appear inverse tendency.

The concentration depth profile through a Cu-rich particle selected from the specimens with different aging times and the proportion of main composition at the centre part of Cu-rich phase particle changing with aging time is shown in Fig.22. It shows that the Cu-rich particle is mainly composed of Cu and also a part of Fe, Cr and Ni when aged for 5h(see Fig.22(a)). The Cu concentration in Cu-rich particle is gradually increasing with aging time, while others composed atoms appear inverse tendency(as shown in Fig.22(b) and (c)). Fig.22(d) shows that Cu content in the Cu-rich segregation area is almost lower than 20at% at early stage of precipitation when Fe is still the mainly composed composition, and then Cu content is increasing continually with aging time and reaches almost 90at% at the centre of Cu-rich particle when aging for 500h. These results represent that Cu atoms gradually concentrate to Cu-rich particles and the other elements(such as Fe, Cr, Ni etc) diffuse away from Cu-rich particles into γ-matrix with the increasing of aging time at 650℃. It may suggest that Cu will be the only main composition in Cu-rich phase when aging for very long time.

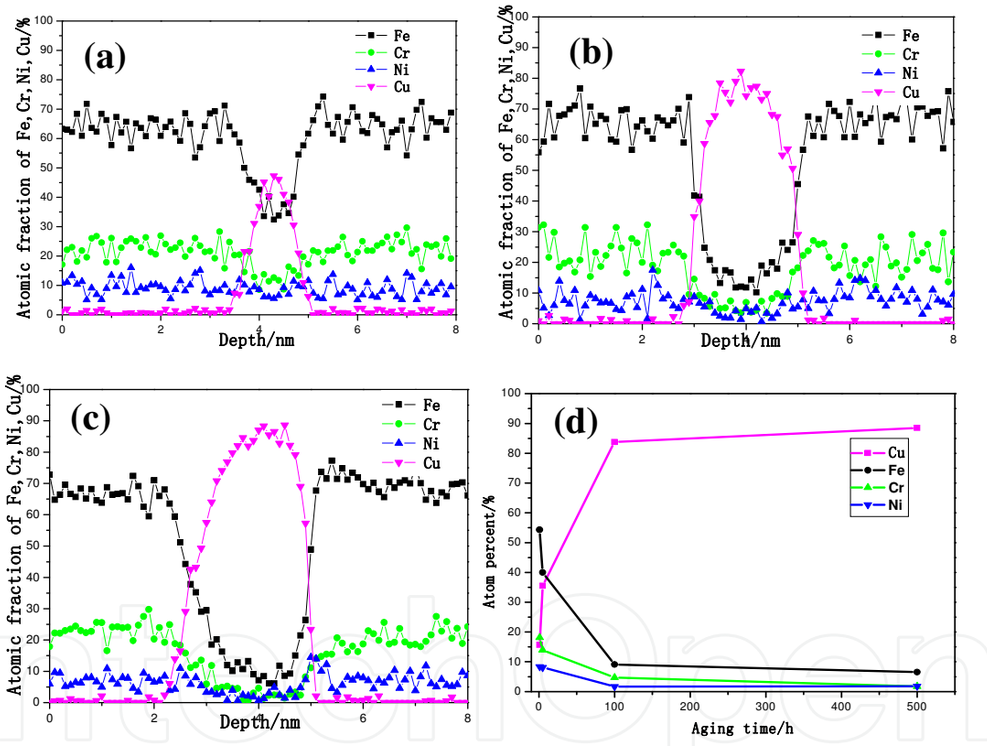

Fig. 22. Concentration depth profile through a Cu-rich particle selected from the specimens aged at 650℃ for different age times, (a)5h, (b)100h, (c)500h and proportion of main composition at the centre part of Cu-rich phase particle changing with aging time(d)

Fig. 23 shows compared results of the atomic reconstruction in a selected area that cut through a Cu-rich particle in Super304H after solid solution treatment and aged for 500h. The depth in the vertical direction is so small that only reflects a few planes of atoms, so it can clearly show the composition through the whole Cu-rich particle. Fig.23(a) shows that all elements distributed homogeneously after solid solution treatment. With the lasting of aging time, much more Cu atoms concentrate into the Cu-rich phase and the other elements

such as Fe, Cr, Ni are rejected from Cu-rich phase into austenitic matrix. It can be seen from Fig.23(b) that Cu atoms are the main atoms in the centre of Cu-rich particle(circled by dashed line), and the other elements are in a very few numbers at 650℃/500h aging. At this time the interphase boundary between Cu-rich phase and austenitic matrix is much clearer than the boundary at the condition of 650℃ aging for 1h only. These results clearly indicate that Cu atoms gradually concentrate into Cu-rich particle and the other elements such as Fe, Cr, Ni diffuse away from Cu-rich phase particle to γ-matrix with the increasing of aging time at 650℃. According to the experimental results, it can suggest that Cu atoms concentrate to form Cu-rich segregation clusters just at the beginning of 650℃ aging, the change from Cu-rich segregated clusters to Cu-rich phase by Cu atom diffusing into the Cu-rich particles and other atoms diffuse to γ-matrix.

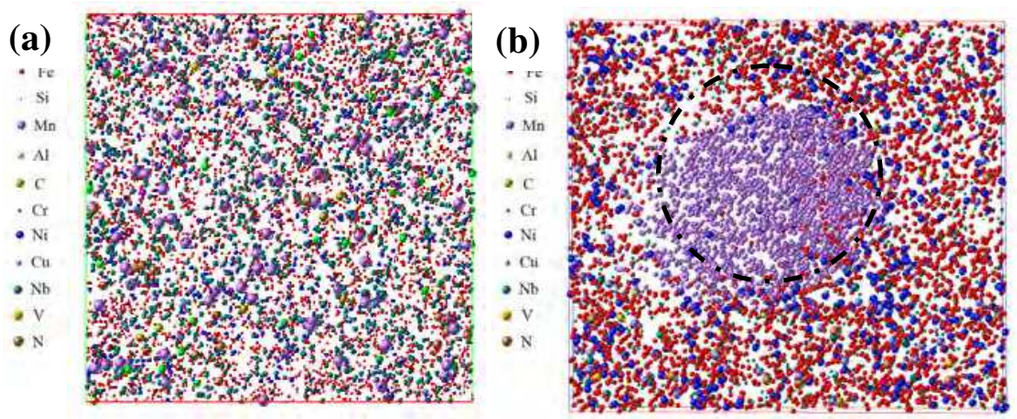

Fig. 23. All elements atomic mapping of Super304H after solid solution treatment(size of selected box is 10nm×10nm×1nm)(a) and aged at 650℃ for 500h (size of selected box is 10nm×9nm×1nm) (b)

4.2.5 The relationship between Cu-rich phase formation and Cu content in Super304H heat-resistant steel

As described in above paragraph, Cu-rich phase is the main strengthening phase in Super304H steel, and Cu atom gradually becomes the main composed element in Cu-rich phase. It means that content of Cu added in Super304H can develop the precipitation of Cu-rich phase, resulting in a strong strengthening effect. Thermal-calc software can be used to predict the formation of Cu-rich phase with different Cu content.

The equilibrium diagrams of Super304H steels with different Cu content calculated by Thermal-calc software are shown in Fig.24. Fig.24(a) is the equilibrium diagram of Super304H steel with 1% Cu. It shows that Cu atoms all dissolve in γ -matrix and Cu-rich phase can not form at 650℃. When the addition of Cu increases to 3%, Cu-rich phase can form at 650℃. Its mole fraction is higher than MX phase which is another strengthening phase precipitates in grains. The mole fraction of Cu-rich phase at equilibrium condition is increasing with the increase of Cu content, and will be more than $M_{23}C_6$ phase as shown in Figure.24(c). Although more Cu addition will induce more Cu-rich phase precipitate which is good for high temperature strength. However, the steel with too much Cu content do not have the best performance in the view point of high temperature ductility(Tan et al., 2010).

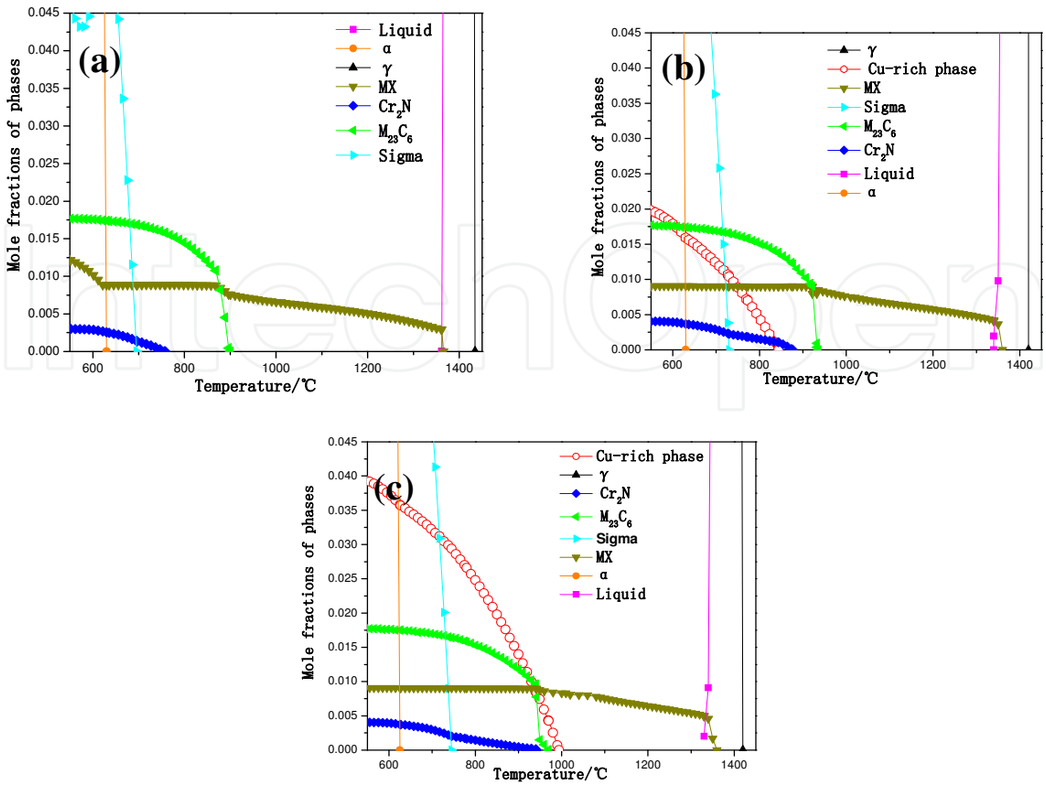

Fig. 24. Equilibrium diagrams of Super304H steels with different Cu content calculated by Thermal-calc software: (a)1%Cu, (b)3%Cu, (c)5%Cu

4.3 HR3C heat-resistant steel

HR3C steel is a kind of austenitic heat-resistant steels. HR3C steel containing with higher chromium(25%Cr) and nickel(20%Ni) is developed to improve corrosion and oxidation resistant properties both for high temperature application. Because of good structure stability of HR3C steel, it characterizes with good high temperature mechanical properties，corrosion/oxidation resistance and weldability for long-term service. It has been also used as superheater/reheater tubes for ultra-supercritical power plant boilers, especially in final stage of reheater tubes.

The chemical composition of HR3C steel for this study is as follows(in mass%): 0.06C, 0.55Si, 0.97Mn, 0.022P, 0.001S, 19.82Ni, 25.23Cr, 0.46Nb, 0.20N, bal. Fe. Its heat treatment is solid solution treated at high temperature 1200-1250℃. According to the service environment of HR3C steel—the highest temperature of reheater tubes, the aging temperature of this steel was selected at 650℃ and 700℃. Long-time aging treatments reach 3,000h-5,000h in order to analyze micro-structure evolutions of HR3C steel.

4.3.1 Long-term mechanical properties

The Vickers micro-hardness of all specimens with aging time at 700℃ have been shown in Fig.25. At initial aging stage the Vickers micro-hardness increases rapidly with aging time.

At 1,000h, the Vickers micro-hardness of the steel has got the maximum. After that, with further aging till 5,000h the hardness still keeps at a high level of 255HV. It is clear that age hardening effect of HR3C steel develops by strengthening phase precipitation.

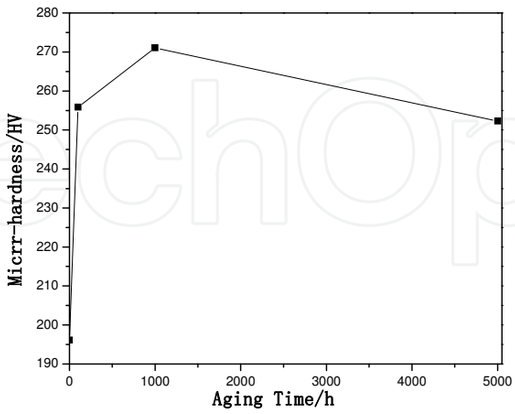

Fig. 25. Micro-hardness of HR3C steel at 700℃ long-term aging

The impact property of HR3C heat-resistant steel at 700℃ is shown in Fig. 26. At the initial aging, impact property decreases dramatically with aging time. The value of impact toughness decreases to 7J at 700℃/300h from 220J at solution condition. But it can keep in a stable level for long time aging till 3,000h. Therefore, the impact property of HR3C steel needs to be improved after long-term aging at 700℃.

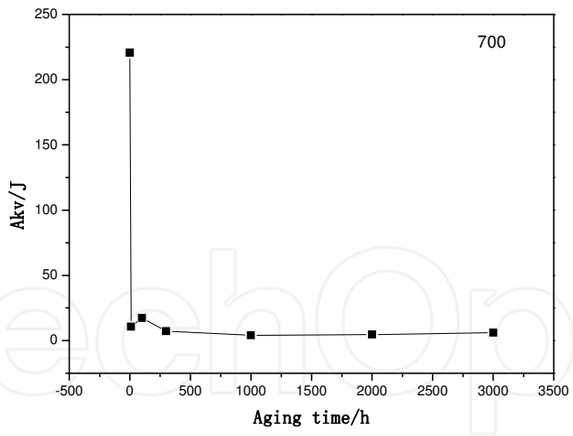

Fig. 26. The impact property changes with aging time at 700℃ in HR3C

4.3.2 Micro-structure analyses

Fig. 27 shows SEM images and EDS of HR3C steel after 500h and 3,000h long-term aging at 650℃. Fig.27 (a) and (b) are the SEM images after 500h and 3,000h aging at 650℃ respectively. Fig. 27 (c), (d) and (e) are EDS results of γ-matrix and precipitated particles in grains, and at grain boundaries respectively. There are several kinds of precipitates in grains and at grain boundaries after long-term aging. $M_{23}C_6$ carbide containing with Cr precipitates

at grain boundaries and NbCrN phase containing with high Nb and Cr precipitates in grains, as shown in Fig. 27(c), (d) and (e).

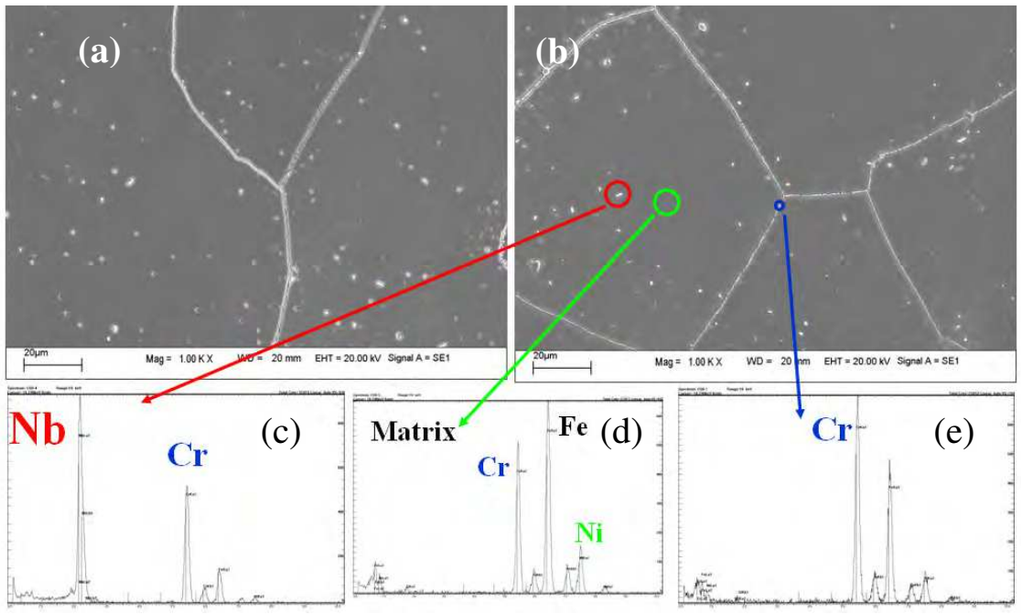

Fig. 27. SEM images of HR3C after aging at 650℃ for (a) 500h and (b) 3,000h, EDS results of (c) the particle in grains, (d) matrix and (e) the particles at grain boundaries

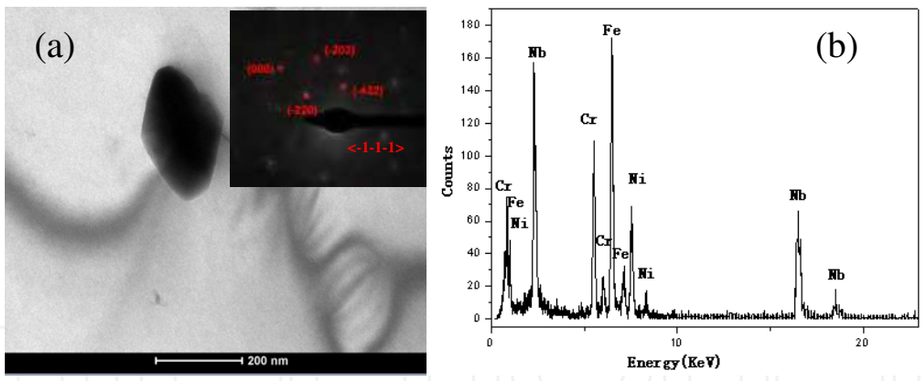

Fig. 28. TEM image of HR3C at solution treatment(a) precipitation with diffraction patterns and (b) EDS

Fig. 28 shows TEM images, diffractions pattern and EDS results of HR3C steel after solid solution treatment condition. MX phase exits in grains at solid solution treatment. Its crystallographic structure is NaCl type(a= 0.4331nm). This kind of MX phase contains with Nb and its size is about 300nm.

Fig. 29 shows TEM images, EDS and diffraction of $M_{23}C_6$ carbides after 3,000h aging at 650℃ in HR3C. $M_{23}C_6$ phase can also precipitate in grains(but mainly at grain boundaries) after long-term aging. Its crystallographic structure is complicated face-center cube. Its lattice parameter is about three times than that of austenite matrix.

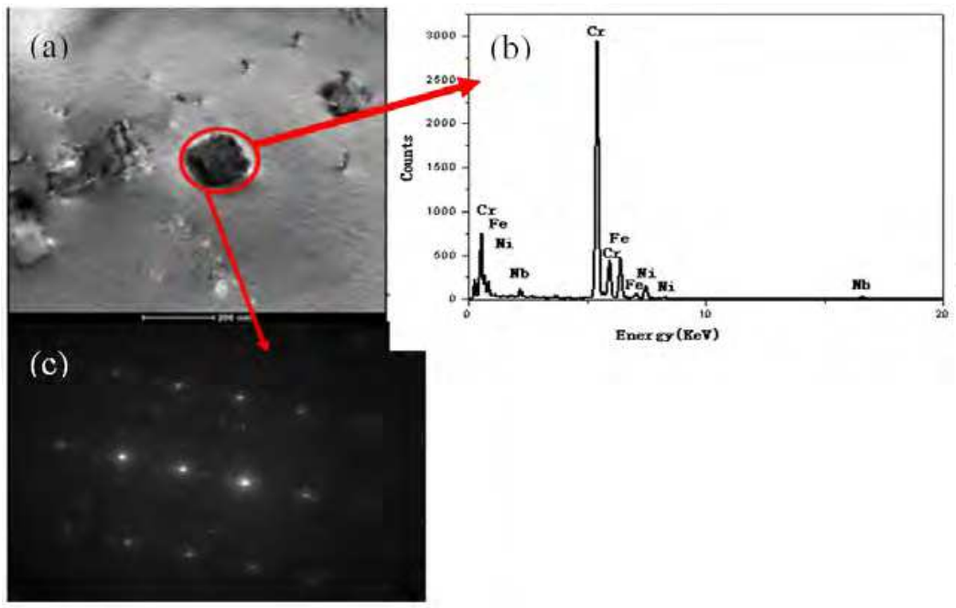

Fig. 29. TEM images of $M_{23}C_6$ carbides after aging 3,000h at 650℃ in HR3C(a) $M_{23}C_6$ carbides (b) EDS and (c) diffraction patterns

4.3.3 The relationship between thermal equilibrium phases and the contents of Nb, N and C in HR3C heat-resistant steel

According to the results and the reported literature(Iseda et al., 2008), the main precipitated phases in HR3C steel are NbCrN phase, $M_{23}C_6$ carbides and σ phase. NbCrN phase and $M_{23}C_6$ carbides play an important role on strengthening effect. However, the brittle σ phase is harmful for mechanical properties at high temperatures. The relationship between thermal equilibrium phases (NbCrN phase, $M_{23}C_6$ carbides and σ phase) and elements (C, N and Nb) in HR3C heat-resistant steel are evaluated by thermodynamic calculation.

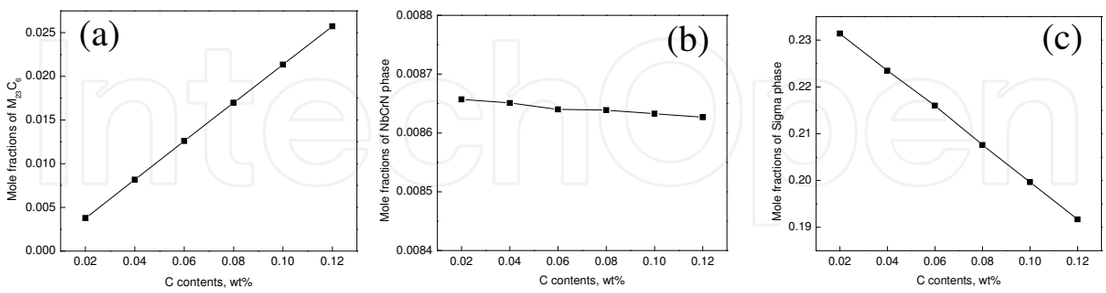

Fig. 30. Effect of C content on mole fractions of $M_{23}C_6$ phase (a), NbCrN phase (b) and σ phase (c) in HR3C steel at 650℃

Fig. 30 shows the effect of C content on mole fractions of $M_{23}C_6$ phase, NbCrN phase and σ phase in HR3C steel, respectively. The mole fractions of $M_{23}C_6$ phase increase in a straight line tendency with C content increasing, shown in Fig. 30(a). For every increasement of 0.02%C content, the mole fractions of $M_{23}C_6$ phase increase 0.5%. Fig.30(b) shows that the

mole fractions of NbCrN phase keep in a stable value with C content increasing. The mole fractions of σ phase decrease in a straight line tendency with C content increasing, shown in Fig. 30(c). With the content of C increasing from 0.02% to 0.12%, the mole fractions of σ phase decrease from 0.23 to 0.19.

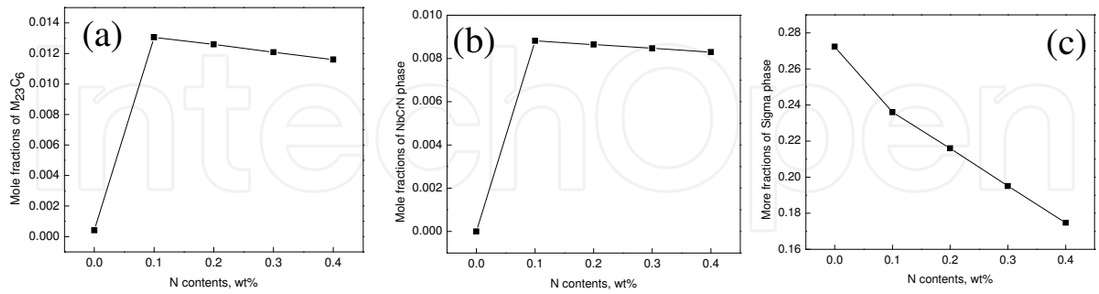

Fig. 31. Effect of N content on mole fractions of $M_{23}C_6$ phase (a), NbCrN phase (b) and σ phase (c) in HR3C steel at 650℃

Fig. 31 shows the effect of N content on mole fractions of $M_{23}C_6$ phase, NbCrN phase and σ phase in HR3C steel, respectively. It is obviously to know that the tendency between the mole fractions of $M_{23}C_6$ phase and N content is similar to that of the mole fractions of NbCrN phase. The mole fractions of $M_{23}C_6$ phase and NbCrN phase both increase quickly with N content increasing from 0 to 0.1%. But the mole fractions of $M_{23}C_6$ phase and NbCrN phase both decrease very slowly with N content increasing from 0.1% to 0.4%, shown in Fig.31(a) and (b). The mole fractions of σ phase decrease very quickly with the increasing of N content. When the N content increases to 0.4%, the mole fractions of σ phase decreases from 0.27 to 0.17, shown obviously in Fig.31(c).

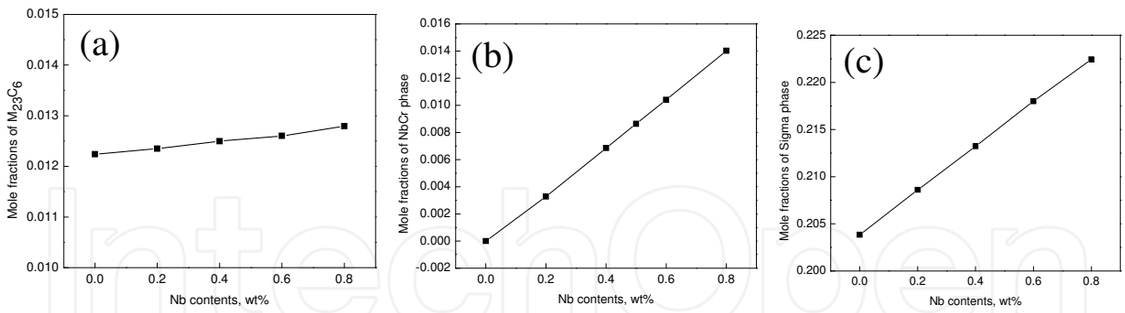

Fig. 32. Effect of Nb content on mole fractions of $M_{23}C_6$ phase (a), NbCrN phase (b) and σ phase (c) in HR3C steel at 650℃

Fig. 32 shows the effect of Nb content on mole fractions of $M_{23}C_6$ phase, NbCrN phase and σ phase in HR3C steel at 650℃. The mole fractions of $M_{23}C_6$ phase increase very slowly with Nb content increasing, shown in Fig.32(a). The mole fractions of the strengthening phase NbCrN and the brittle σ phase both increase with the increasing of Nb content. For every increasement of 0.2%Nb content, the mole fractions of NbCrN phase and σ phase increase 0.4% and 0.5%, respectively shown in Fig.32(b) and (c). Thus, the Nb content should be controlled in a correct level for reducing Sigma phase in order to get good strengthening effect and to avoid embrittlement.

From these results obtained by experimental observation and thermodynamic calculation, advanced austenitic heat resistant steels are strengthened by second phase precipitation. High Cr and Ni containing HR3C heat resistant steel is the candidate material for high terminal superheater/reheater components in USC fossil power plants with higher steam parameters on the view point of corrosion and oxidation resistance. However, it is a little insufficient in high temperature stress rupture strength. Cu addition in austenitic heat resistant steel is effective to develop nano-size Cu-rich phase precipitation during high temperature long-term service, which causes an excellent high temperature strengthening effect and also good microstructure stability. Cu-rich phase precipitates in Super304H heat resistant steel is a good example. In order to improve the strength of 25Cr-20Ni type austenitic heat resistant steel, the addition of Cu to induce Cu-rich phase precipitation is strongly suggested. So the further development of austenitic heat resistant steels may contain high content of Cr and Ni to meet the requirement of corrosion/oxidation resistance and coupled with nano-size MX, Cu-rich phase in the grains for second phase precipitation strengthening and to add B for stabilization $M_{23}C_6$ phase precipitates at grain boundaries.

5. Conclusion

The development of advanced austenitic heat resistant steels is promoted by the progress of USC fossil power plants, which urgently needs new materials with high temperature strength and good corrosion/oxidation resistant properties for superheater/reheater components. In this chapter three advanced austenitic heat resistant steels widely used for 600℃ USC power plants, TP347H, Super304H and HR3C, have been investigated by SEM, TEM and 3DAP technologies coupled by thermodynamic calculation. Results show that high temperature strength of these three heat resistant steels is mainly dependent on fine second phase precipitation during long-term aging. The MX phase mainly precipitates in the grains and $M_{23}C_6$ phase mainly precipitates at grain boundaries. The Cu-rich phase precipitates in grains characterize with outstanding precipitation strengthening effect for Super304H in comparison with TP347H and HR3C. This is also the main reason why Super304H gains superior high temperature strength. According our research results we conclude as follow:

1. In TP347H austenitic heat resistant steel, some primary NbC as inclusions with 1～3μm in size randomly distribute in grains and sometimes also at grain boundaries at solid solution treatment condition. There are also some undissolved NbC particles with about 200nm in size in the grains. After long-term aging at 650℃, the Nb rich MX type phase intensively precipitates in grains and there are also some $Cr_{23}C_6$ precipitates at grain boundaries. These very fine high Nb containing MX phase precipitates during long time aging and keeps in nano-size contribute to good strengthening effect on TP347H steel. The calculated results show that the amount of MX phase increases with increasing of C/N and Nb contents. The amount of σ phase decreases with the increasing of C content. Adding 0.2%N to this steel, MX phase contains N, Nb, Cr with a certain amount of C, which is a complex carbon nitride and makes excellent strengthening effect.
2. In Super304H austenitic heat resistant steel, there are about 3% Cu-rich phase and 0.38% MX in volume fraction precipitate in grains. Elaborate analyses conducted by unique 3DAP technology show that Cu atoms are soluted in matrix after high temperature solid solution treatment and have formed austenitic matrix with high saturation of Cu. Cu-rich segregated clusters in 2nm size contained about 20at% Cu can

be quickly formed just after 650℃ aging for 1h. The average size of Cu-rich segregation clusters are increasing slowly with aging time. The concentrations of Cu atom in Cu-rich segregation clusters are continuously increasing and simultaneously the atoms of Fe, Cr and Ni are defusing to γ-matrix. In result of that Cu becomes the main composition of Cu-rich phase. However, there are still some other elements in the Cu-rich phase after long time aging. In fact, Cu-rich phase is not a pure Cu phase. The precipitation character of Cu-rich phase is different from ε-Cu phase precipitation in ferritic steels. It is defined that when the Cu-rich particle contains more than 50at% Cu to be called Cu-rich phase. The copper element has almost concentrated to 90at% in the center part of Cu-rich phase after 500h aging. It is clearly shown that the formation of Cu-rich phase from Cu-rich segregated clusters has been completed.

Cu-rich phase grows slowly during 650℃ aging and can keep in nano-size for very long aging. The average size of Cu-rich phase is only about 35nm at 650℃ aging even for 10,000h. The density of Cu-rich phase particles is very high and can reach to $0.38\times10^{14}/m^2$ after long-term aging at 650℃ for 10,000h. Cu rich phase characterizes with fine nano-size, high density distribution and low growth rate and it is also the largest volume fraction among all the precipitates in Super304H. Homogeneously distributed fine Cu-rich phase can effectively block dislocation moving for excellent strengthening effect. It is clearly confirmed that this kind of nano-size Cu-rich phase is the most important precipitation strengthening phase in Super304H.

3. In HR3C austenitic heat resistant steel, the main equilibrium phases are NbCrN, $M_{23}C_6$, MX, σ and Cr_2N according to Thermal-Calc results. The amounts of NbCrN and σ phase increase with the increasing of Nb content. There are a lot of phases precipitate in the grains and at grain boundaries during 650℃ long time aging by experimental observation. Among these phase the main dispersive precipitates are NbCrN, MX and $M_{23}C_6$ phase. NbCrN phase and MX phase precipitated in grains. $M_{23}C_6$ carbides precipitated mainly at grain boundaries and it can also precipitated partially in grains. During long-term high temperature service a brittle phase (σ phase) may precipitate which will degrade mechanical properties .

6. Acknowledgment

This project is supported by China National Natural Science Foundation under the grant No:50931003. Authors would like also to thank Profs Bangxin Zhou and Wenqing Liu who work in Instrumental Analysis & Research Center, Shanghai University for their guidance on 3DAP experiments and valuable discussion on the results.

7. References

Ayer, R.; Klein, C. F. & Marzinsky, C, N. (1992). Instabilities in stabilized austenitic stainless steels. *Metall Mater Trans,* 1992, Vol.23A, (May 1991), pp.2455-2467

Blum, R.; Vanstone, R, W and Messelier-Gouze, C. (2004). Materials Development for Boilers and Steam Turbines Operating at 700℃, *Proceedings to the Fourth International Conference on Advances in Materials Technology for Fossil Power Plants* , Hilton Head Island, South Carolina, U.S., October 25-28, 2004

Chen, Q, R.; Stamatelopolous, G, N. Helmrich, A. Heinemann, J. Maile, K. & Klenk, A. (2007). Materials Qualification for 700℃ Power Plants, Fifth International Conference on Advances in Materials Technology for Fossil Power Plants, U.S., October 3-5, 2007

Chi, C, Y.; Dong, J, X. Liu, W, Q. & Xie, X, S. (2010). 3DAP investigation of precipitation behavior of Cu-rich phase in Super304H heat resistant steel. *Acta Metallurgica Sinica,* Vol.46, No.9, (Sept 2010), pp.1141-1146

Gibbons, T, B. (2009). Superalloys in modern power generation applications. *Materials Science and Technology,* Vol.25, No.2, (July 2008), pp.129-135

Hong, H, U.; Rho, B, S. & Nam, S, W. (2001). Correlation of $M_{23}C_6$ precipitation morphology with grain boundary characteristics in austenitic stainless steel. *Materials Science and Engineering A,* 2001, Vol.318, (Jan 2001), pp. 285–292

Hughes, A.; Dooley, B. & Paterson, S. (2003). Oxide Exfoliation of 347HFG in High Temperature Boilers, *7th International Conference and Exhibition on Operating Pressure Equipment,* Sidney, Australia, April 2-4, 2003

Igarashi, M. (2004). Development of 18-8 steel (Super304H) having high elevated temperature strength for fossil fired boilers. *CAMP-ISIJ*, 2004, Vol.17, pp. 336-340

Igarashi, M.; Okada, H. & Semba, H. (2005). Development of 18-8 steel (Super304H) having high elevated temperature strength for fossil fired boilers, *Proceedings 9th Workshop on the Innovative Structural Material for Infrastructure in 21st Century,* NIMS, Tsukuba, 2005

Iseda, A.; Okada, H. Semba, H. & Igarashi, M. (2007). Long term creep properties and microstructure of SUPER304H, TP347HFG and HR3C for A-USC boilers. *Energy Mater,* Vol.2, No.4, (August 2008), pp. 199-206

Komai, N.; Igarashi, M. Minami, Y. Mimura, H. Masuyama, F. Prage, M. & Boyles, P, R. (2007). Field test results of newly developed austenitic steels in the Eddystone Unit No.1 boiler, *Proceedings of CREEP8 Eighth International Conference on Creep and Fatigue at Elevated Temperatures,* San Antonio, Texas, U.S., July 22-26, 2007

Lin, F. S.; Cheng, S. C. & Xie, X. S. (2008). Ultrasupercritical power plant development and high temperature materials applications in China. *Energy Mater,* Vol.3, No.4, (October 2009), pp. 201-207

Liu, Z, D.; Xie, X, S. Cheng, S, C. Lin, F, S. Wang, Q. J. & Xu, S. Q. (2011). The research and development of advanced boiler steels used for USC power plants, *4th Symposium on Heat Resistant Steels and Alloys for High Efficiency USC Power Plants 2011,* Beijing, China, April 11-13, 2011

Minami, Y.; Kimura, H. & Ihara, Y. (1986). Microstructural changes in austenitic stainless steels during long-term aging. *Materials Science and Technolgoy,* Vol.2 (August 1986), pp. 795-806

Muramatsu, K. (1999). Advanced heat resistant steel for power generation, The university Press, Cambridge

Masuyama, F. (2001). History of Power Plants and Progress in Heat Resistant Steels. *ISIJ Int,* Vol.41, No.6, (December 2000), pp. 612-625

Masuyama, F. (2005). Alloy development and material issues with increasing steam temperature, *Proceedings to the Fourth International Conference on Advances in Materials Technology for Fossil Power Plants* , Hilton Head Island, South Carolina, U.S., October 25-28, 2004

Sawaragi, Y. & Hirano, S. (1992). The Development of a new 18-8 austenitic stainless steel (0.1C-18Cr-9Ni-3Cu-Nb,N) with high elevated temperature strength for fossil fired boilers. Jono, M. & Inone, T. ed. Mechanical Behavior of Materials, Vol.4, London: Pergamon Press, pp. 589-594

Sawaragi, Y.; Ogawa, K. Kato, S. Natori, A. & Hirano, S.(1992). Development of the economical 18-8 stainless steel (Super304H) having high elevated temperature strength for fossil fired boilers. *The Sumitomo Search,* 1992, No.48, (Jan 1992), pp. 50-58

Sawaragi, Y.; Otsuka, N. Senba, H. & Yamamoto, S. (1994). Properties of a new 18-8 austenitic steel tube(Super304H) for fossil sired boilers after service exposure with high elevated temperature strength. *The Sumitomo Search,* 1994, No.56, (Oct 1994), pp.34-43

Sourmail, T. (2001). Precipitation in creep resistant austenitic stainless steels. *Materials Science and Technology,* 2001, Vol.17, (Jan 2001), pp. 1-14

Senba, H.; Sawaragi, Y. Ogawa, K. Natori, A. & Kan, T. (2002). The development of high efficiency 18-8 type Super304H tube used in USC power plants. *Materia Jpn,* 2002, Vol.41, pp. 120-125

Sourmail, T. & Bhadeshia, H, K, D, H. (2005). Microstructural evolution in two variants of NF709 at 1023 and 1073K. *Metall Mater Trans,* 2005, Vol.36A,(Feb 2004), pp.23-34

Tanaka, H.; Muruta, M. Abe, F. & Irie, H. (2001). Microstructural evolution and change in hardness in type 304H stainless steel during long-term creep. *Materials Science and Engineering A,* 2001, Vol.(319–321), pp. 788–791

Tan, S. P.; Wang, Z, H. Cheng, S, C. Liu, Z, D. Han, J, C. & Fu, W, T. (2010), Effect of Cu on Aging Precipitation Behavior of Cu-Rich Phase in Fe-Cr-Ni Alloy. *Journal of Iron and Steel Research, International,* 2010, Vol.17, No.5, (Mar 2009) pp.63-68

Viswanathan, R. & Bakker, W. (2001). Materials for Ultrasupercritical coal power plants-Boiler Materials: Part 1. *J Mater Eng Perform,* Vol.10, No.1, (February 2001), pp. 81-95

Viswanathan, R. (2004). Materials technology for coal-fired power plants. *Advanced Materials & Processes,* (August 2004), pp. 73-76

Viswanathan, R.; Henry, J, F. Tanzosh, J. Stanko, G. Shingledecker, J. Vitalis, B. & Purgert, R. (2005). U.S. Program on Materials Technology for Ultra-Supercritical Coal Power Plants. *J Mater Eng Perform,* Vol.14, No.3, (June 2005), pp. 281-292

Viswanathan, R.; Coleman, K. & Rao, U. (2006). Materials for ultra-supercritical coal-fired power plant boilers. *International Journal of Pressure Vessels and Piping,* 2006, Vol. 83, pp. 778-783

Viswanathan, R.; Shingledecker, J. Hawk, J. & Goodstine, S.(2009) Advanced Materials for Use Ultrasupercritical Coal Power Plants, *2009 Symposium on Advanced Power Plant Heat Resistant Steels and Alloys,* Shanghai, China. Oct, 2009

Xie, X, S.; Chi, C, Y. Yu, H, Y. Yu, Q, Y. Dong, J, X. Chen, M, Z. & Zhao, S, Q.(2010). Structure Stability Study on Fossil Power Plant Advanced Heat-Resistant Steels and Alloys in China. *Advances in Materials Technology for Fossil Power Plants Proceedings from the Sixth International Conference,* Santa Fe, New Mexico, USA. August, 2010

Yoshikawa, K.; Teranishi, H. Tokimasa, K. Fujikawa, H. Miura, M. & Kubota, K. (1988). Fabrication and properties of corrosion resistant TP347H stainless steel. *J. Mater. Eng,* Vol.10, No.1, (1988), pp. 69-84

Yu, H, Y.; Dong, J, X. & Xie, X, S. (2010). 650℃ long-term structure stability study on 18Cr-9Ni-3CuNbN heat-resistant steel. *Mater. Sci. Forum,* Vol. 654-656, (2010), pp.118-121

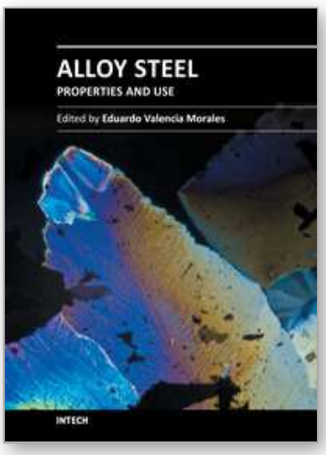

Alloy Steel - Properties and Use

Edited by Dr. Eduardo Valencia Morales

ISBN 978-953-307-484-9
Hard cover, 270 pages
Publisher InTech
Published online 22, December, 2011
Published in print edition December, 2011

The sections in this book are devoted to new approaches and usages of stainless steels, the influence of the environments on the behavior of certain classes of steels, new structural concepts to understand some fatigue processes, new insight on strengthening mechanisms, and toughness in microalloyed steels. The kinetics during tempering in low-alloy steels is also discussed through a new set-up that uses a modified Avrami formalism.

How to reference

In order to correctly reference this scholarly work, feel free to copy and paste the following:

Chengyu Chi, Hongyao Yu and Xishan Xie (2011). Advanced Austenitic Heat-Resistant Steels for Ultra-Super-Critical (USC) Fossil Power Plants, Alloy Steel - Properties and Use, Dr. Eduardo Valencia Morales (Ed.), ISBN: 978-953-307-484-9, InTech, Available from: http://www.intechopen.com/books/alloy-steel-properties-and-use/advanced-austenitic-heat-resistant-steels-for-ultra-super-critical-usc-fossil-power-plants

INTECH
open science | open minds

InTech Europe
University Campus STeP Ri
Slavka Krautzeka 83/A
51000 Rijeka, Croatia
Phone: +385 (51) 770 447
Fax: +385 (51) 686 166
www.intechopen.com

InTech China
Unit 405, Office Block, Hotel Equatorial Shanghai
No.65, Yan An Road (West), Shanghai, 200040, China
中国上海市延安西路65号上海国际贵都大饭店办公楼405单元
Phone: +86-21-62489820
Fax: +86-21-62489821

IntechOpen